



Morris, C., Glennie, S., Lam, H., Baum, H., Kandage, D., Williams, N., Morgan, D., Woolfson, D., & Davidson, A. (2019). A Modular Vaccine Platform Combining Self-Assembled Peptide Cages and Immunogenic Peptides. *Advanced Functional Materials*, 29(8), [1807357].
<https://doi.org/10.1002/adfm.201807357>

Peer reviewed version

Link to published version (if available):
[10.1002/adfm.201807357](https://doi.org/10.1002/adfm.201807357)

[Link to publication record in Explore Bristol Research](#)
PDF-document

This is the author accepted manuscript (AAM). The final published version (version of record) is available online via Wiley at <https://onlinelibrary.wiley.com/doi/10.1002/adfm.201807357>. Please refer to any applicable terms of use of the publisher.

University of Bristol - Explore Bristol Research

General rights

This document is made available in accordance with publisher policies. Please cite only the published version using the reference above. Full terms of use are available:
<http://www.bristol.ac.uk/red/research-policy/pure/user-guides/ebr-terms/>

Article type: Full paper

vSAGE: a modular vaccine platform combining self-assembled peptide cages and immunogenic peptides

*Caroline Morris, * Sarah J. Glennie, Hon S. Lam, Holly E. Baum, Dhinushi Kandage, Neil A.*

Williams, David J. Morgan, Derek N. Woolfson and Andrew D. Davidson**

Dr. C. Morris, Dr. H. E. Baum, Prof. D. N. Woolfson

BrisSynBio, University of Bristol, Bristol BS8 1TQ, UK

School of Chemistry, University of Bristol, Bristol BS8 1TS, UK

E-mail: D.N.Woolfson@bristol.ac.uk; caroline.morris@bristol.ac.uk

Dr. S. J. Glennie, Mr. H. S. Lam, Miss. D. Kandage, Dr. H. E. Baum, Prof. N. A. Williams, Dr. D.

J. Morgan, Dr. A. D. Davidson

School of Cellular and Molecular Medicine, University of Bristol, Bristol BS8 1TD, UK

E-mail: andrew.davidson@bristol.ac.uk

Prof. D. N. Woolfson

School of Biochemistry, University of Bristol, Bristol BS8 1TD, UK

ORCID

Caroline Morris: 0000-0002-4797-0317

Holly E. Baum: 0000-0002-1311-6446

Derek N. Woolfson: 0000-0002-0394-3202

Andrew D. Davidson: 0000-0002-1136-4008

Keywords: coiled coil, peptide design, self-assembly, subunit vaccine, synthetic biology.

Contributions

DNW, NAW and ADD conceived the project. CM, SJG, NAW, DJM, DNW and ADD planned the experiments. CM designed, synthesized and characterized the peptides. SJG conducted the experiments for Figures 3-6. DK performed critical preparatory experiments for those in Figure 7. HSL and HEB conducted the experiments for Figure 7. All authors assisted in reading and preparation of the manuscript.

Abstract

Subunit vaccines use delivery platforms to present minimal antigenic components for immunization. The benefits of such systems include multivalency, self-adjuvanting properties and more specific immune responses. Previously, we have reported the design, synthesis and characterization of self-assembling peptide cages (SAGEs). In these, *de novo* peptides are combined to make hubs that assemble into nanoparticles when mixed in aqueous solution. Here we show that SAGEs are non-toxic particles with potential as accessible synthetic peptide scaffolds for the delivery of immunogenic components. To this end, SAGEs functionalized with the model antigenic peptides tetanus toxoid₆₃₂₋₆₅₁ and ovalbumin₃₂₃₋₃₃₉ drive antigen-specific responses both *in vitro* and *in vivo*, eliciting both CD4⁺ T cell and B cell responses. Additionally, SAGEs functionalized with the antigenic peptide hemagglutinin₅₁₈₋₅₂₆ from the influenza virus are also able to drive a CD8⁺ T cell response *in vivo*. This work demonstrates the potential of SAGEs to act as a modular scaffold for antigen delivery, capable of inducing and boosting specific and tailored immune responses.

1. Introduction

Vaccines have been pivotal to the development of modern medicine, from general childhood vaccination to the global eradication of smallpox and near elimination of polio. Nonetheless, successful vaccines for major targets such as malaria and human immunodeficiency virus (HIV) have yet to be established,^[1] and the recent Zika virus outbreak highlights the need for ongoing vaccine development.^[2] Related to this, there is a global rise in antimicrobial resistance, and so relying on medication alone to treat a disease once contracted is not a guaranteed option.^[3] Thus, continued vaccine development is still an important area of both basic and applied research.^[4]

Traditional vaccines, based on the administration of killed or attenuated organisms or their purified components, have proven to be amongst the most effective methods for disease prevention.^[5] However, a number of safety issues relating to the production and administration of

these vaccines limit their universal application, including: the risk of reversion to a virulent organism; decreased or altered immune response after inactivation; the possibility of causing disease in immune compromised individuals; and the requirement to maintain the cold chain.^[6]

Recent advances in the identification of single components (antigens) capable of generating protective immunity has driven the development of subunit vaccines, where instead of using whole pathogens, specific portions are delivered using a scaffold.^[7] Furthermore, improved genetic methods and expression systems have resulted in cheaper and large-scale production of recombinant microbial antigens without the need to culture highly pathogenic infectious agents.^[8]

Despite these advantages, recombinant subunit vaccines are often less immunogenic than their traditional whole-organism counterparts. To overcome decreased immunogenicity, subunit vaccines require the addition of immunostimulatory agents, i.e. adjuvants,^[9] or optimization of delivery systems that specifically target immune cells and tailor immune responses.^[10] Another key strategy for subunit vaccine design is to create a multivalent platform enabling the expression of multiple antigens in a repetitive array.^[11] Having a delivery system with several copies of T- and B-cell antigens from different strains of the pathogen could generate cross-protective immunity and increase the immunogenicity of the vaccine. If required, these platforms could be adapted to display both antigens and immunopotentiators, such as Toll-like receptor (TLR) agonists,^[12] thus enhancing the activity, uptake and presentation of antigens to the immune system. Adopting strategies that direct antigen delivery and release may stimulate more potent immune responses using lower doses of weak immunogens. Reducing the need for the prime and boost strategies often required in conventional vaccination regimens would lead to dose-sparing, beneficial for reducing development cost and improving immunization efficiency schedules in the event of vaccine shortages.^[13]

Subunit vaccine delivery systems typically include the use of liposomes,^[14] virus-like particles^[15] or peptide nanoparticles.^[16] The rationale is that these mimic the size and shape of viruses to simulate an immune response similar to a live attenuated vaccine, whilst maintaining the selectivity of a subunit vaccine. Protein engineering and design approaches, in particular, provide

increased synthetic access and control of components,^[17] with one example being the self-assembling protein nanoparticle (SAPN) platform.^[18] SAPNs comprise trimeric and pentameric α -helical coiled-coil motifs linked in a single peptide. These polypeptides assemble into particles approximately 20 nm in diameter. They have been optimized to act as vaccine carriers, and their biodistribution *in vivo* has been monitored.^[19] They can serve as repetitive antigen displays capable of inducing a variety of immune responses, and include particles modified with epitopes derived from severe acute respiratory syndrome coronavirus,^[20] malaria,^[21] HIV^[22] and influenza virus.^[12b] Other peptide-based self-assembling systems with potential as functionalized structures take on the form of nanofibers, or tubes, rather than resembling viral capsid architecture.^[23] These assemblies exploit the thermal stability^[24] and environmental responsiveness^[25] of synthetic peptide systems, along with dose control^[26] and the incorporation of whole-protein antigens.^[27] Such examples demonstrate the potential of synthetic peptide- and protein-based vaccine delivery platforms.

The work described herein explores the potential of self-assembling peptide cages (SAGEs) to act as modular scaffolds in a synthetic biology approach for antigen delivery. SAGEs are made from *de novo* α -helical coiled-coil peptides. Specifically, a set of homotrimeric (CC-Tri3) and heterodimeric (CC-Di-A and CC-Di-B) peptides are linked *via* a disulfide bond to form two complementary hubs.^[28] Mixing of these hubs in aqueous solution leads to co-assembly into hexagonal lattices,^[29] ultimately folding into spherical particles approximately 100 nm in diameter (**Figure 1a**). The working hypothesis of SAGE architecture is that each CC-Tri3 unit is oriented within the peptide lattice such that its *N* terminus faces the exterior of the particle and its *C* terminus faces the interior, while CC-Di-A and CC-Di-B have greater freedom of rotation around the disulfide bond.^[28, 30] Subsequently, functionality can be incorporated *via* CC-Tri3 to allow for bespoke dose delivery as the antigen dose is controlled *via* peptide synthesis and conjugation rather than passive encapsulation.^[31] The fully synthetic SAGE appears to withstand relatively robust functionalization,^[31a] can be predictably modified to alter cellular uptake,^[31b] and the modularity of the system allows for fine control of modification.^[29]

SAGEs are potentially an alternative platform for developing subunit vaccines with the following advantages. Their modularity means that by mixing different ratios of the hub building blocks we can incorporate multiple antigens, thus tailoring the immune response. Furthermore, the nature of the SAGE structure provides a multivalent platform which can potentially be used to deliver multiple antigens from different strains, thereby increasing antigen immunogenicity. Another important consideration is component stability. The hub building blocks can be lyophilized and stored as powder long-term, which could also be a benefit to such a platform by avoiding problems associated with the cold chain. Here, we investigate this potential of the SAGE scaffold as a vaccine platform, and whether SAGEs functionalized with model antigenic peptides successfully deliver them to drive specific immune responses. The results show that SAGEs are non-toxic and capable of enhancing the immune responses, *in vitro* and *in vivo*, against model antigenic peptides.

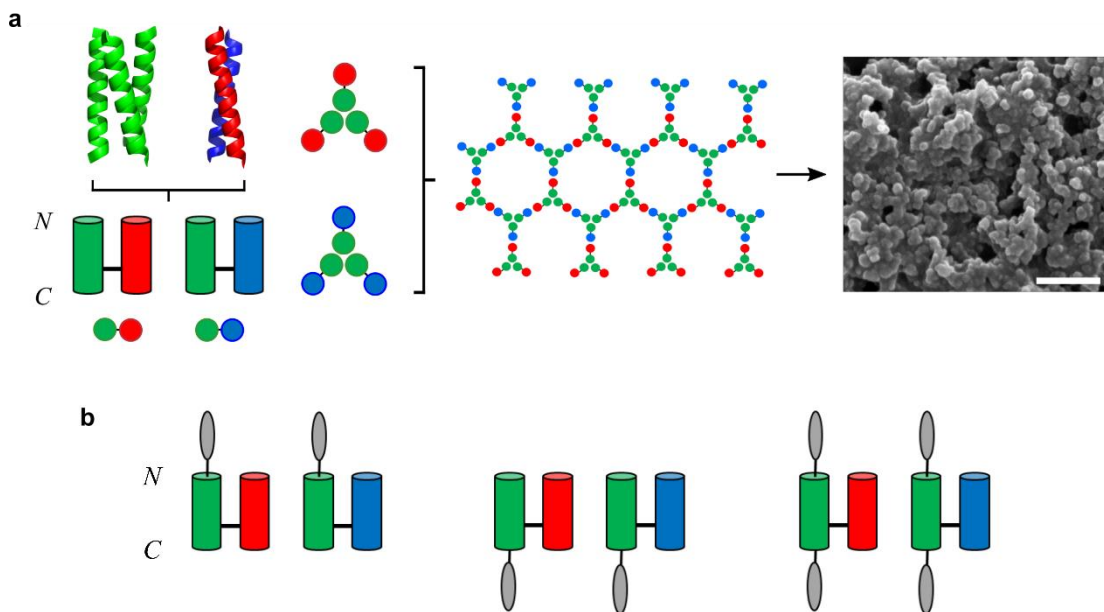


Figure 1: SAGE assembly and design of functionalized hubs. **a** Schematic representation of parent SAGE assembly. Linking the heterodimer to the homotrimer forms complementary hubs that, when mixed, self-assemble into a lattice and close to form particles approximately 100 nm in diameter (as observed by scanning electron microscopy (SEM); scale bar = 1 μ m). **b** Cartoons representing incorporation of different model antigenic peptides into hubs. Model antigenic peptides (grey ovals) can be incorporated either *N*- or *C*-terminal to the trimer, or at both termini.

2. Results and Discussion

2.1. SAGEs are robust to modification with antigenic peptides

SAGEs were functionalized with model antigenic peptides (epitopes). This was achieved by extending the CC-Tri3 peptide sequences with the epitopes during solid-phase peptide synthesis (SPPS). SAGEs were designed and synthesized with this functionality added at either the *N* or *C* terminus, or both termini of CC-Tri3 (Figure 1b, Tables S1-3, Figures S1-6). For *in vitro* work we used the model antigenic peptide tetanus toxoid₆₃₂₋₆₅₁ (TT),^[32] a CD4⁺ T cell epitope. *In vivo* experiments used the model antigenic peptides ovalbumin₃₂₃₋₃₃₉ (OVA),^[33] a CD4⁺ T cell and B-cell epitope, and influenza virus A/PR/8/34 (H1N1) hemagglutinin₅₁₈₋₅₂₆,^[34] a CD8⁺ T cell epitope. For this last epitope a short, *N*-terminal 10-residue sequence from the herpes simplex virus DNA polymerase was included to maximize effective proteasomal processing and presentation by major histocompatibility receptor class I (MHC-I) molecules.^[35] It was this extended peptide (HA) that was used for additional *in vivo* experiments. The functionalized CC-Tri3 peptides were subjected to biophysical characterization before being conjugated with the CC-Di-A/B peptides to make hubs.

First, circular dichroism (CD) spectroscopy was used to test for any impact on the trimeric component of all functionalized trimers. To monitor the helicity of each functionalized peptide, the mean residue ellipticity (MRE, deg cm² dmol⁻¹ res⁻¹) at 222 nm was recorded as spectra. The observed signals were consistent with folded CC-Tri3 appended with unfolded peptides (**Figure 2a**, Table S4). Peptide stability was not greatly altered, as observed by comparable midpoint of unfolding temperatures during thermal denaturation experiments (Figure 2b, Table S4). Functionalized hubs were similarly assessed and found to be unaffected (Figure S7 and Table S5).

All functionalized CC-Tri3 peptides were then analyzed using sedimentation velocity analytical ultracentrifugation (AUC; Figure S8). The predominant peak in the TT- and HA-functionalized peptides was trimeric, with TT-CC-Tri3-TT peptide showing an additional smaller species. The OVA-functionalized peptides did not appear to form discrete trimers in solution, and

so whilst their thermal stability was not drastically altered it is possible that the addition of OVA affected the ability of the peptide to trimerize.

The assembly of functionalized SAGE particles was assessed by scanning electron microscopy (SEM) and dynamic light scattering (DLS). By SEM, TT-functionalized SAGEs produced particles of comparable size to parent SAGEs, SAGE-HA formed slightly larger particles, and OVA-functionalized SAGEs formed much larger particles (Figure 2c-h). The data obtained from DLS measurements often gave a range of particle sizes within samples and it was not possible to determine particle size from these experiments (Figure S9). While the hydrodynamic diameter increased compared to that of the individual hubs, this technique demonstrated the ability of these particles to form aggregates. For both of these techniques the aggregation of the sample meant it was not possible to accurately determine particle size.

However, overall, this suite of biophysical characterization confirms that SAGEs can be modified with model antigenic peptides and competently self-assemble into particles.

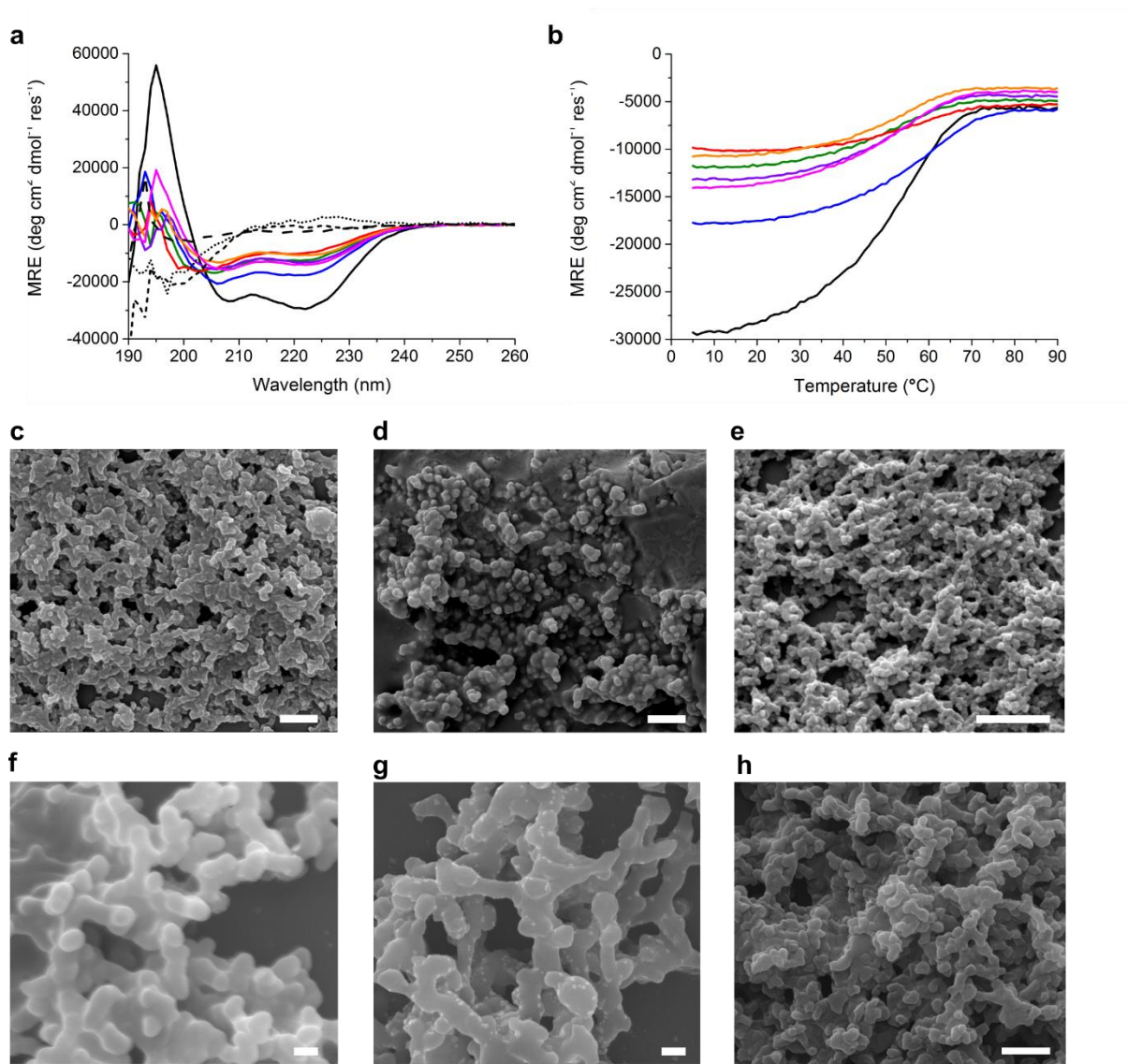


Figure 2: Biophysical characterization of functionalized SAGEs. **a-b** CD spectroscopy of functionalized CC-Tri3 peptides (CC-Tri3 in black, TT-CC-Tri3 in blue, CC-Tri3-TT in green, TT-CC-Tri3-TT in red, OVA-CC-Tri3 in purple, CC-Tri3-OVA in orange, CC-Tri3-HA in pink) and antigenic peptides (TT in black lines, OVA in black dashes, HA in black dots). 5 °C wavelength (**a**) and thermal denaturation curves (**b**) of functionalized CC-Tri3 and antigenic peptides. Conditions: 50 μM peptide in PBS (pH 7.4). **c-h** SEM images of assembled functionalized SAGEs: TT-SAGE (**c**), SAGE-TT (**d**), TT-SAGE-TT (**e**), OVA-SAGE (**f**), SAGE-OVA (**g**), SAGE-HA (**h**). Conditions: 50 μM peptide in PBS (pH 7.4); 1 h assembly; deposited onto Si wafer on an SEM stub; scale bar 1 μm.

2.2 Parent SAGEs are non-toxic and stimulate PBMC proliferation.

In vitro studies of SAGE uptake by HeLa cells showed them to be non-toxic,^[31b] and so SAGE toxicity with other cell types was assessed using human peripheral blood mononuclear cells (PBMCs) isolated from whole blood. PBMCs were exposed to the polyclonal stimulus

phytohemagglutinin (PHA) to induce a response indicative of T cell proliferation, in the presence or absence of SAGE. PBMCs were able to proliferate in response to PHA irrespective of SAGE concentration, confirming that the assembled particles are not toxic (**Figure 3a**). To assess whether SAGE were intrinsically immunogenic, resting PBMCs were cultured with parent SAGE at a range of concentrations to determine if proliferation was induced. PBMC proliferation was observed at all concentrations, with higher SAGE concentrations giving the greatest proliferative response (Figure 3b). The ability of the SAGEs to stimulate PBMC proliferation may be attributed to either weak inherent immunogenicity or mitogenicity.

The source of this proliferation was further probed by assaying the SAGE components, both the building blocks (HubA and HubB) and their constituent peptide components (CC-Tri3, CC-Di-A and CC-Di-B). Their ability to stimulate proliferation of PBMCs was assayed (Figure 3c) along with an immunological memory response in human and mouse sera (Figure 3d-e). The proliferative response to SAGEs was not found to be due to any particular peptide component. We posit that SAGEs may induce this response due to their shape, size and local concentration. From these results, it is proposed that the ability of SAGEs to prompt low-level immune responses would be beneficial for their development as a vaccine delivery platform, potentially in a similar manner to that employed by conjugate vaccines.^[36]

SAGE toxicity *in vivo* was also assayed by immunizing mice with extreme doses of parent SAGE. BALB/c mice were immunized with four doses (350 µg) of parent SAGE, each dose at an interval of three weeks (two weeks for the final immunization). Serum aspartate aminotransferase (AST) levels, used to evaluate liver function, were comparable between SAGE-immunized (five mice) and control (PBS only, three mice) animals (Figure 3f), and immunization did not lead to an alteration in percentage lymphocyte and monocyte population numbers in peripheral blood (Figure S10). Immunized mice did not develop any injection site reactions or adverse systemic effects, and in combination with the lack of histopathological changes (Table S6) these data suggest SAGEs are not toxic *in vivo*.

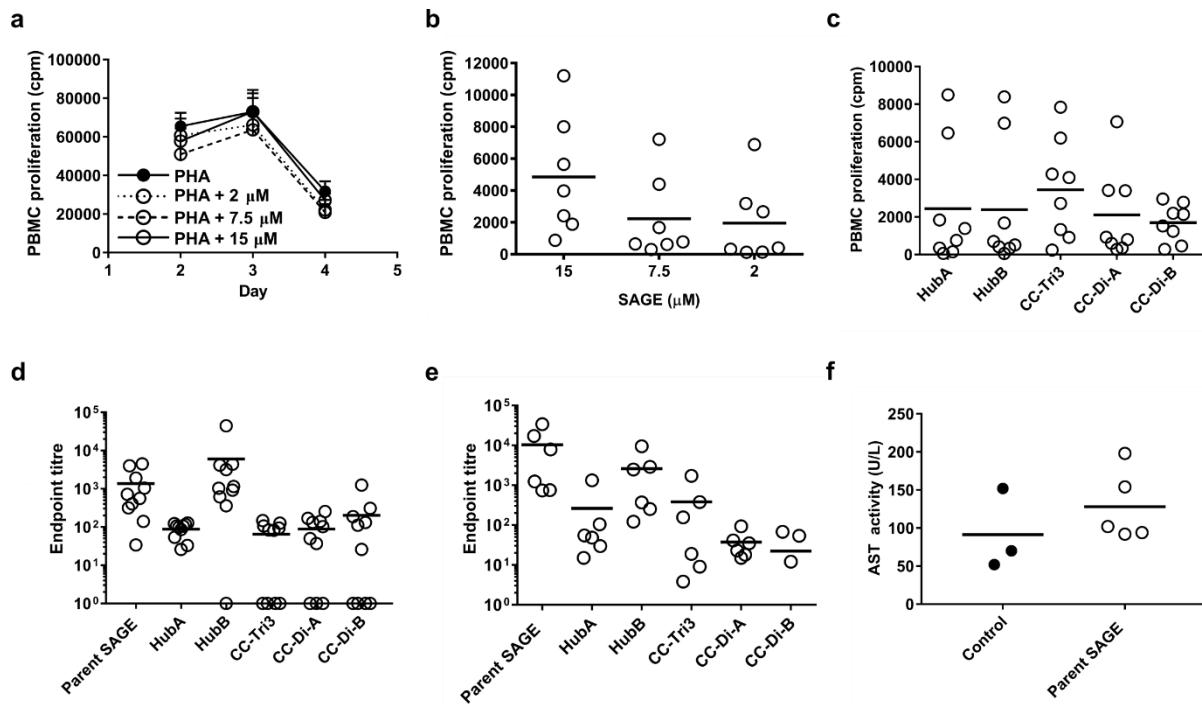


Figure 3: Parent SAGEs are non-toxic and stimulate PBMC proliferation. **a** PBMC proliferation in response to exposure to the polyclonal stimulus PHA and increasing amounts of SAGE to assay SAGE toxicity. Conditions: 15 μM (solid line), 7.5 μM (dashed line) and 2 μM (dotted line) SAGE in PBS (pH 7.4) with PHA; 10 $\mu\text{g ml}^{-1}$ PHA alone as positive control (filled circles); proliferation measured by the incorporation of ^3H -thymidine, in counts per minute (cpm); $n = 4$ donors. **b** Peak PBMC proliferative response upon exposure to parent SAGEs alone to assay SAGE immunogenicity. Conditions: 15, 7.5 and 2 μM SAGE in PBS (pH 7.4); proliferation measured as before (cpm); $n = 7$ donors. **c** Peak PBMC proliferative response upon exposure to SAGE components when incubated at 37 $^{\circ}\text{C}$ for up to 10 days. Conditions: Components at 7.5 μM in PBS (pH 7.4); proliferation measured as before (cpm); $n = 8$ donors. **d** Endpoint titre of antibody in human sera recognizing parent SAGE and components. $n = 10$ donors. **e** Endpoint titre of antibody in mouse sera recognizing parent SAGE and components. $n = 6$. **f** *In vivo* mouse toxicity data for parent SAGEs as analyzed by AST levels. BALB/c mice were immunized subcutaneously with four sequential doses of SAGE (350 μg in PBS (pH 7.4), $n = 5$ mice) or PBS ($n = 3$ mice) at three week intervals (two weeks for the final immunization).

2.3 Antigen presenting cells internalize but are weakly activated by parent SAGEs

Antigen presenting cells (APCs) are immune phagocytes that internalize, process and present foreign material to other immune cells. After establishing that parent SAGEs are non-toxic but potentially immunogenic/mitogenic, we explored whether immune phagocytes internalize and are primed by SAGE particles. Human PBMCs were purified and differentiated into monocyte-derived dendritic cells (MDDCs) and macrophages (MDMs). To monitor the cellular uptake of particles,

5 % of the hub building blocks were replaced with fluorescently labelled counterparts to assemble FITC-SAGE (Tables S1-3). Cellular uptake was quantified by flow cytometry, isolating internalized fluorescence by quenching external fluorescence with trypan blue (**Figure 4**). Both MDDCs and MDMs took up SAGEs with similar kinetics, with the greatest rate of uptake in the first 60 minutes. However, MDMs had a greater overall uptake of SAGEs compared to MDDCs. Although MDDCs and MDMs are both known to be phagocytic cells, the uptake of nanoparticles can be influenced by particle size and aggregation state and additionally, the maturation state of the cells,^[37] which may explain the differences in SAGE uptake observed.

Next, we investigated whether phagocytes were activated after SAGE uptake as determined by the increased secretion of a range of cytokines and the increased surface expression of co-stimulatory and antigen presenting molecules. MDDCs and MDMs were cultured with SAGEs, followed by the analysis of cell-surface markers and cytokines in the cell-culture supernatants. Cytokine secretion by MDDCs and MDMs was not induced by SAGEs, whilst treatment of the cells with the positive control of lipopolysaccharide (LPS) increased the amounts of TNF- α , IL-6, IL-1 β , IL-10, IL-12p70 and IL-1 α secreted (Figure S11a). Whilst phagocytic cells were shown to upregulate the co-stimulatory molecule CD80, and MHC class I and II expression was observed, these effects were moderate in comparison to the effects of LPS (Figure S11b).

In combination, these experiments confirm that both MDMs and MDDCs internalize SAGE particles and are weakly activated by them, demonstrating the potential of SAGEs as a delivery platform for a vaccine.

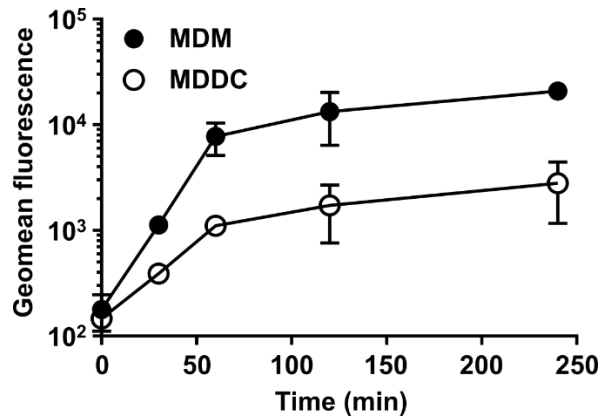


Figure 4: Parent SAGEs are internalized by antigen presenting cells. Uptake of fluorescently labelled parent SAGEs by MDDCs (open circles) or MDMs (filled circles) quantified by flow cytometry. Conditions: 10 μ M ^{FITC}SAGE in PBS (pH 7.4); n = 2 donors.

2.4 TT-functionalized SAGEs drive a CD4⁺ T cell response *in vitro*

We tested whether TT-functionalized SAGE would alter phagocytic uptake and downstream antigen-specific responses using PBMCs and flow cytometry as before. Compared to the previous experiment (Figure 4) we observed enhanced uptake of the parent SAGE by MDMs (**Figure 5a**), most likely due to donor variability. ^{FITC}SAGE-TT were taken up as effectively as parent SAGEs after 120 min, while TT-^{FITC}SAGE and TT-^{FITC}SAGE-TT were taken up significantly less well by this timepoint (**Figure 5a**). By the final timepoint, constructs with TT functionality at the N-terminus of CC-Tri3 were internalized by MDDCs less rapidly than those functionalized at the C-terminus. Consistent with our working model for SAGE assembly and structure, if the surface of the particle has been altered by the N-terminal modifications this has possibly affected particle uptake by MDDCs.

To test whether differences in uptake of functionalized SAGE affected downstream antigen-specific responses, the proliferative ability of human PBMCs was determined after exposure to each of the three TT-functionalized SAGEs for up to seven days (Figure 5b). PBMC proliferation is indicative of a T cell response and, in this case, considered to be a CD4⁺ T cell response against the TT peptide, a model CD4⁺ T cell epitope.^[38] Experimental controls of parent SAGE, free TT

peptide, and parent SAGE mixed with free TT peptide elicited low levels of cellular proliferation. TT-SAGE and SAGE-TT have an equivalent amount of TT as both parent SAGE + TT and free TT peptide in the controls. The amount of SAGE peptide is equivalent for all constructs and controls, and so TT-SAGE-TT has double the amount of TT relative to its singly functionalized counterparts. Two of the constructs, TT-SAGE-TT and SAGE-TT, induced a significantly greater proliferative response than free TT peptide. The doubly functionalized TT-SAGE-TT induced higher proliferative responses than those singly functionalized, though this difference was not significant. Here, the *N*-terminal functionality in TT-SAGE-TT is suspected of affecting its internalization. Despite delivering the same dosage, there was a significant difference in the response to TT-SAGE and SAGE-TT. We conclude that the less effective uptake of TT-SAGE impacts the downstream antigen-specific proliferative response.

The results of these *in vitro* experiments confirm that APCs are able to internalize functionalized SAGEs, and to drive a downstream antigen-specific response. These data provide the first evidence that SAGEs have potential as vaccine scaffolds delivering antigenic components.

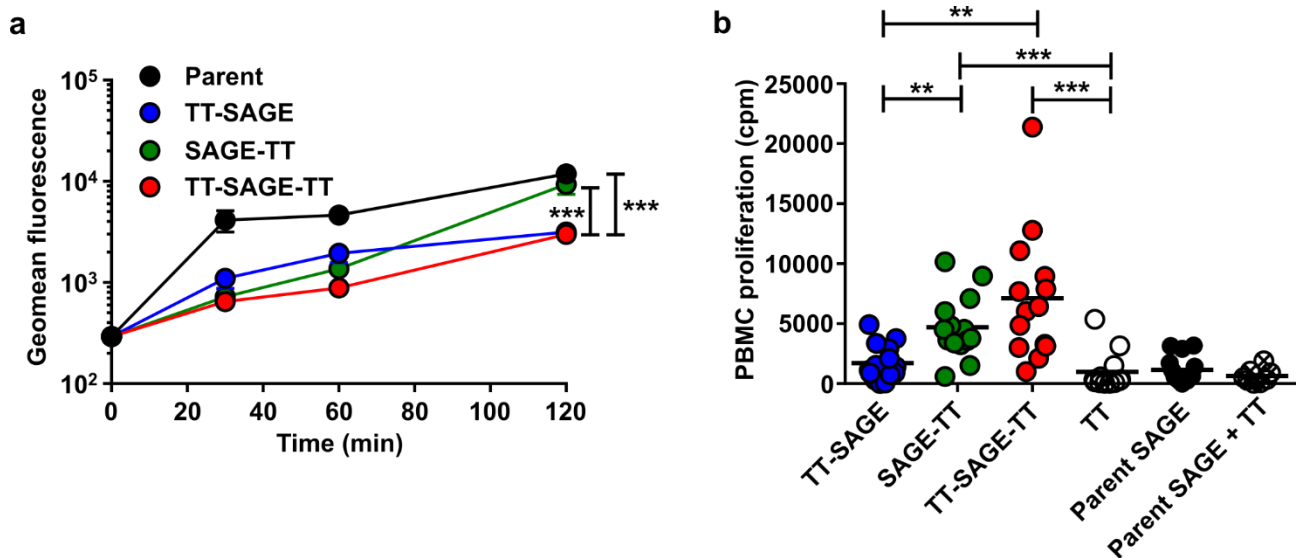


Figure 5: TT-functionalized SAGEs drive an antigen-specific response *in vitro*. **a** Uptake of fluorescently labelled parent (black) and TT-functionalized SAGEs (TT-^{FITC}SAGE in blue, ^{FITC}SAGE-TT in green, TT-^{FITC}SAGE-TT in red) by MDDCs quantified by flow cytometry. Conditions: 10 μ M ^{FITC}SAGE in PBS (pH 7.4); n = 6 donors. **b** Peak proliferative response of PBMCs to TT-functionalized SAGEs compared to a range of controls (free TT peptide in open circles, parent SAGE in black, parent SAGE mixed with free TT peptide in crossed circles) over a period of 10 days. Conditions: 7.5 μ M TT-functionalized SAGE and equivalent control conditions in PBS (pH 7.4); n = 14 donors. ** P < 0.01, *** P < 0.001.

2.5 OVA-functionalized SAGEs drive CD4⁺ T cell and antibody responses *in vivo*

Before testing for an antigen-specific response *in vivo*, the immunogenicity of parent SAGEs in an animal model was assessed by immunization in a prime/boost regimen. Groups of BALB/c mice were either immunized with 25 μ g of parent SAGE at day 0 (d0) or day 0 and day 21 (d0 + d21), before assaying splenocyte proliferation and antibody titres. Animals immunized with a booster dose of SAGE showed an increased proliferation of SAGE-specific splenocytes when restimulated *ex vivo* with SAGE particles (Figure 6a). Furthermore, the prime/boost regimen also generated a significant increase in the production of anti-SAGE antibodies following a single immunization (Figure 6b). Based on these results, experiments with functionalized SAGEs were also performed with a prime/boost regimen in order to bolster the desired immune response.

OVA-functionalized SAGEs were designed and synthesized to contain either N- or C-terminal epitopes. Following the promising results observed with TT-SAGE-TT, two copies of the OVA epitope were conjugated to CC-Tri3 to increase the delivered dose. BALB/c mice were

primed on d0 and boosted on d21 with a 160 µg dose of OVA, either in the form of OVA-functionalized SAGE or free OVA peptide. The free peptide was delivered both with and without Complete Freund's Adjuvant (CFA), in addition to a further control group immunized with parent SAGE. Splenocyte proliferation was monitored as a measure of T cell proliferation,^[39] in this case that of CD4⁺ T cells in response to the OVA antigen. Splenocytes from mice given SAGE in any form were able to generate an anti-SAGE proliferative response when restimulated with SAGE *ex vivo* (Figure 6c) and produced anti-SAGE antibodies (Figure 6d). A low-level anti-SAGE antibody response was also observed in mice immunized with OVA + CFA, despite not receiving SAGE in any form. We believe this was due to the use of the adjuvant, resulting in an overall higher concentration of antibodies in the sera, and in turn a low level of non-specific binding. In parallel, splenocytes were also restimulated *ex vivo* with OVA peptide (Figure 6e). Mice given free OVA peptide with CFA mounted the strongest anti-OVA proliferative response, which is expected from the use of the adjuvant. However, the response against free OVA peptide without CFA was enhanced by immunizing with an equivalent dose in the form of OVA-functionalized SAGE particles. Mice given OVA-functionalized SAGE also produced OVA-specific antibodies (Figure 6f). Whilst the positive control of free OVA peptide with CFA generated the greatest antibody titres, OVA-functionalized SAGE gave a significantly greater response than the free OVA peptide. This result demonstrates the potential of the SAGE system as a delivery platform capable of enhancing an immune response when compared to equivalent amounts of the free immunogenic peptide.

A greater response, both in terms of CD4⁺ T cell proliferation and antibody production, was observed when OVA was delivered as part of a functionalized SAGE than as a free peptide. While OVA-SAGE stimulated a stronger CD4⁺ T cell proliferative response (Figure 5e), SAGE-OVA stimulated greater antibody production (Figure 5f). Whilst these results are contradictory, OVA-functionalized SAGES improve the antigen-specific response relative to free OVA peptide in both cases

These experiments demonstrate the effective uptake and processing of functionalized SAGEs *in vivo*, driving an antigen-specific response. The ability to drive both a CD4⁺ T cell and antibody response shows further promise for SAGEs as a vaccine delivery system.

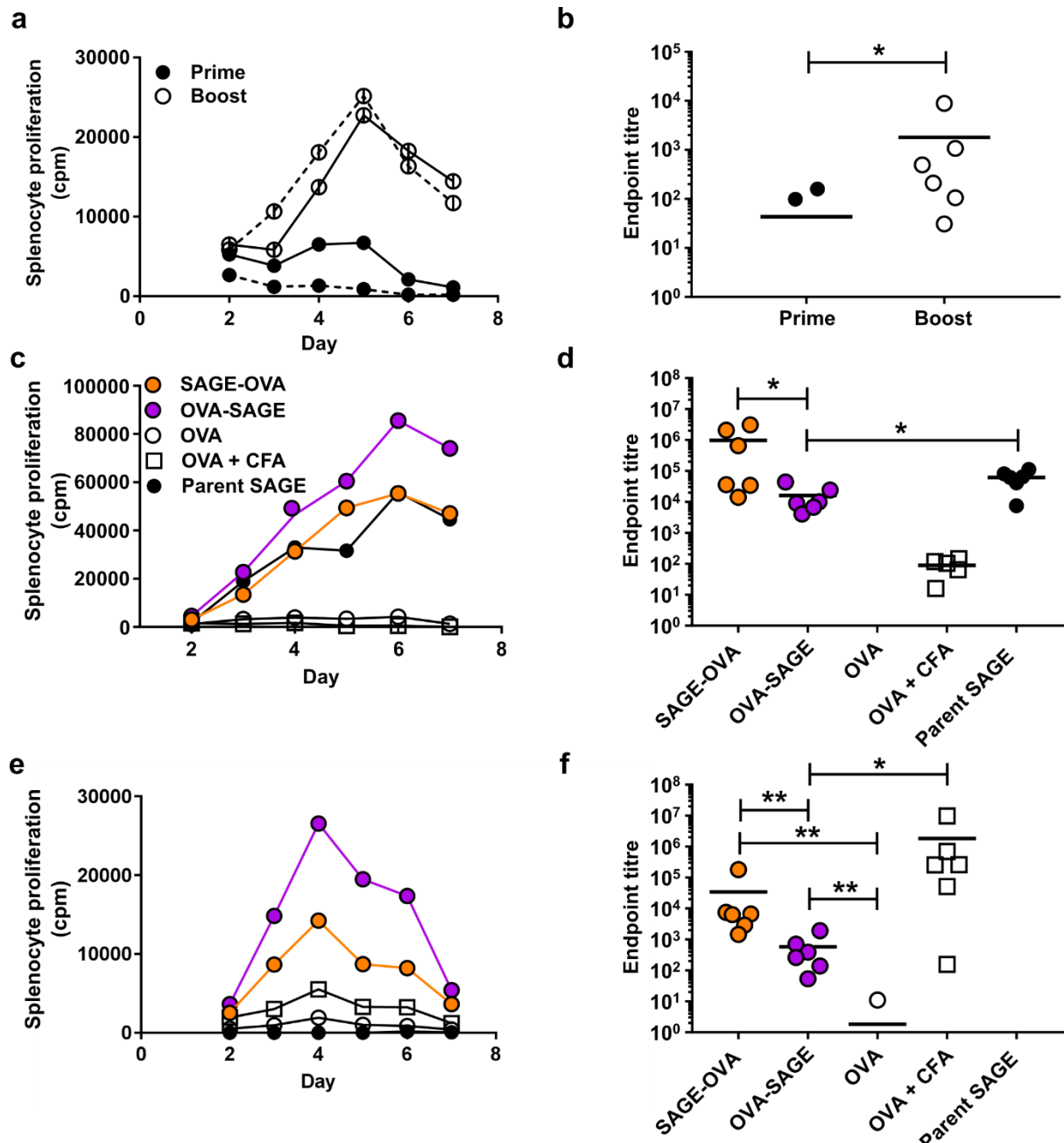


Figure 6: Parent SAGEs benefit from a prime/boost immunization schedule, and OVA-functionalized SAGEs drive an antigen-specific response *in vivo*. **a** Proliferation of murine splenocytes after either a single (prime, filled circles) or booster (boost, open circles) immunization of parent SAGE. $n = 6$ mice (2 groups of 3, solid and dashed lines). **b** EPT ELISA using parent SAGE as antigen to monitor antibody production in the prime (closed circles) and boost (open circles) groups. **c** Proliferation of murine splenocytes isolated after booster immunizations, restimulating *ex vivo* with parent SAGE. **d** EPT ELISA using parent SAGE as antigen to monitor anti-SAGE antibody production. **e** Proliferation of murine splenocytes isolated after booster immunizations, restimulating *ex vivo* with OVA peptide. **f** EPT ELISA using OVA peptide as antigen to monitor anti-OVA antibody production. **a-b** $n = 6$ mice, each immunized with 25 μg of parent SAGE in PBS (pH 7.4) in a prime/boost schedule (d0 and d21). **c-f** $n = 6$ mice, each immunized with 160 μg of OVA either in the form of functionalized SAGE or free peptide in PBS (pH 7.4) in a prime/boost schedule (d0 and d21). Parent SAGE control at equivalent amount to OVA-functionalized SAGE conditions. Immunization with SAGE-OVA (orange), OVA-SAGE (purple), OVA peptide (open circles), OVA peptide + CFA (open squares) or parent SAGE (filled circles). * $P < 0.05$, ** $P < 0.01$.

2.6 SAGE-HA drives a CD8⁺ T cell response *in vivo*

Next, SAGEs were functionalized with the MHC class I epitope to test whether or not this platform could also enhance priming of naïve CD8⁺ T cell responses *in vivo*. Transgenic mice were used to test for this response to SAGEs functionalized with the extended HA.^[40] SAGEs were functionalized with a single copy of HA at just the C terminus of CC-Tri3, as MHC class I processing is more specific than the MHC class II so far tested and positioning of the epitope has more of an effect on processing.^[35] To this end, we utilized transgenic clone 4 (CL4) CD8⁺ T cells, which express a high-affinity T cell receptor (TcR) for the HA epitope. Accordingly, magnetic-activated cell sorting (MACS)-purified naïve CL4 CD8⁺ T cells were labelled with the proliferation marker CellTrace[™] Violet (CTV). As the CTV-labelled (CTV-CL4) cells divide after priming, daughter cells will contain less of the label and so will become distinguishable from undivided, fully-labelled unprimed CTV-CL4 cells. Naïve BALB/c mice were injected intravenously (i.v.) with purified CTV-CL4 cells. Mice were simultaneously immunized subcutaneously (s.c.) with either the HA peptide alone or SAGE-HA at 200 nM or 2 µM (delivering 19 ng or 188 ng of HA per mouse, respectively) to establish an appropriate dose. The use of transgenic T cells allowed for greatly reduced doses compared to previous experiments, as these cells are primed to respond to this particular epitope. After 3 days, the CTV-labelled CL4 cells (CTV-CL4) were isolated from the spleens of these mice, and the extent of proliferation was determined by flow cytometric analyses of CTV expression. The data show that in mice immunized with HA peptide alone, CL4 T cells proliferated in response to both concentrations of the peptide. This is evidenced by a shift of CTV-labelled cells to the left of the panel as a result of the loss of CTV (**Figure 7a**). However, in mice immunized with SAGE-HA there was even greater CL4 T cell proliferation, at both concentrations, compared with mice immunized with HA peptide alone. This is evidenced by the appearance of a discrete population of highly-divided cells (**Figure 7a**; left of the dashed line). Indeed, further analyses with either the HA peptide or with SAGE-HA (both at 2 µM) showed that there was a

significant increase in the percentage of these highly-divided cells in mice immunized with SAGE-HA compared with immunization of HA alone (Figure 7b).

These data therefore demonstrate that functionalizing SAGE with the hemagglutinin₅₁₈₋₅₂₆ epitope enhances its delivery *in vivo*.

Collectively, the results obtained using HA- and OVA-functionalized SAGEs show that SAGEs are capable of enhancing a range of different immune responses *in vivo*.

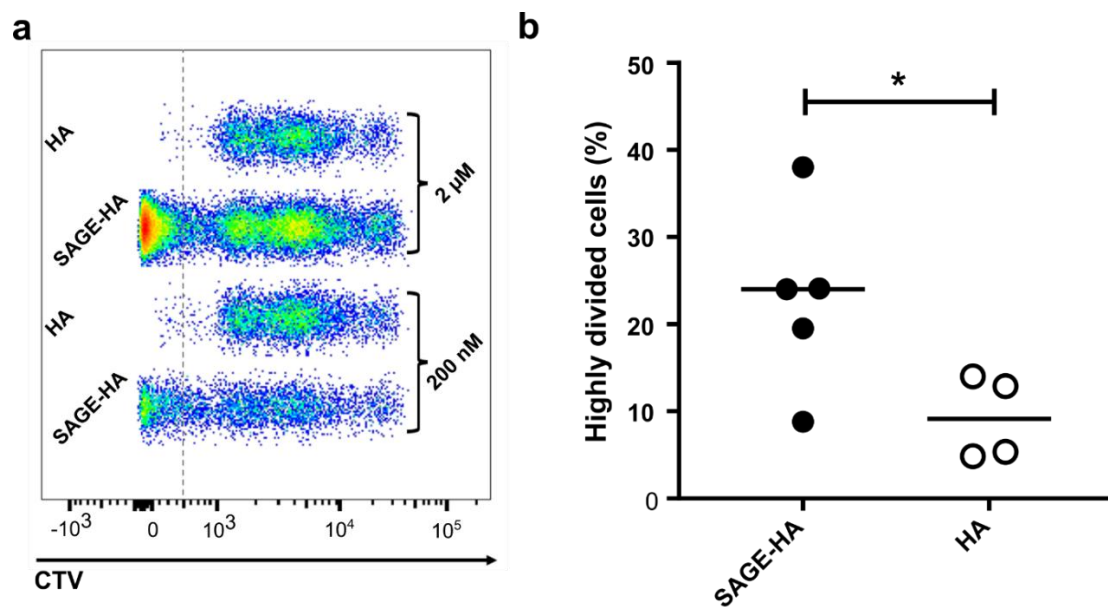


Figure 7: HA-functionalized SAGEs drive a greater CD8⁺ T cell response than equivalent free peptide *in vivo*. **a** Proliferation of CTV-CL4 cells isolated from mice simultaneously immunized with CTV-CL4 cells (3×10^6 cells, 100 μ l i.v.) and HA or SAGE-HA (100 μ l of 200 nM or 2 μ M s.c.). Highly divided cells were determined from cells past the gating threshold (dotted line). $n = 1$ mouse per condition. **b** Percentage of highly divided cells in each mouse immunized with SAGE-HA or HA. Average value for SAGE-HA is $24.0 \% \pm 14.6 \%$, and for HA is $9.1 \% \pm 4.6 \%$. Data from immunization with CTV-CL4 cells (3×10^6 cells, 100 μ l i.v.) and SAGE-HA (filled circles: 100 μ l of 2 μ M s.c., $n = 5$ mice) or HA (open circles: 100 μ l of 2 μ M s.c., $n = 4$ mice). 100 μ l of 200 nM or 2 μ M SAGE-HA delivers 19 ng and 188 ng of HA, respectively. * $P < 0.05$.

3. Conclusion

The work described herein explores one potential application of self-assembling peptide cages (SAGEs), nanoparticles comprising *de novo* α -helical coiled-coil peptides. Subunit vaccines, instead of using the whole pathogen, utilize a scaffold to deliver pathogenic components. The use of SAGEs as such a scaffold offers a synthetic biology approach to subunit vaccine development, where the protein cages can be modified to deliver immunogenic components. The modularity of SAGEs allows for control over dose and delivery, in addition to the possibility of a multivalent system.

We have demonstrated the potential of SAGEs to act as an antigen delivery platform through *in vitro* and *in vivo* toxicity assays, *ex vivo* immunogenic screens, and the use of functionalized SAGEs to probe a range of immune responses against model antigenic peptides.

In vitro experiments using the model tetanus toxoid antigen (TT) confirm that antigen-presenting cells (APCs) are able to internalize functionalized SAGEs, though the positioning of the functionalization may affect uptake. However, importantly, these experiments show that functionalized SAGEs are still internalized by monocyte-derived dendritic cells (MDDCs), and that these particles are effectively processed to drive a downstream antigen-specific CD4⁺ T cell response. In addition, the response to TT-functionalized SAGEs is greater than to an equivalent dose of free TT peptide. Future work looks to improve uptake consistency and enhance downstream responses, including targeting of MDDCs and cleavable linkers.

SAGEs functionalized with the model ovalbumin antigen (OVA) are able to drive stronger immune responses *in vivo* than equivalent amounts of OVA peptide, including both CD4⁺ T cell and B cell responses. However, whilst we have demonstrated the ability to drive an antigen-specific response *in vivo*, our data with OVA-functionalized SAGEs highlight the need to increase the dose of antigen relative to SAGE per immunization. Ongoing work seeks to functionalize SAGEs with antigenic protein components to increase this ratio, so that peptides processed from the antigen rather than the SAGE form the majority of peptides presented at the APC surface. Dose-sparing is an

important consideration for new vaccines to optimize economic and efficient immunization schedules. Further work should investigate the role of SAGE immunogenicity/mitogenicity in the antigen-specific response to establish if a prime/boost regimen is the most appropriate.

We anticipate that to provide protection, the platform must be able to drive a range of immune responses. To build on the observed antigen-specific CD4⁺ T cell and B cell responses, we incorporated a CD8⁺ T cell epitope from the influenza virus hemagglutinin into the SAGE architecture *via* an extended peptide to enhance epitope delivery (HA). By adoptive transfer we assayed the proliferative response of transgenic T cells primed to recognise this epitope. We are encouraged by the increased response relative to free HA peptide and believe that the added ability to enhance a CD8⁺ T cell response gives the system potential as a vaccine scaffold. With further optimization, we anticipate exploiting the modularity of the system to target multiple branches of the immune system to protect against a challenge. This might take the form of particles comprising hubs with multiple antigenic functionalities, or the use of whole protein functionality to increase the immunogenic response. Lyophilization of particles functionalized with whole proteins must then be investigated, as the work described herein has used antigenic peptides, demonstrated to withstand this process.

Positioning of the SAGE functionality and its effect on uptake and, importantly, downstream responses are areas which future work will investigate further. Based on the stricter processing of MHC class I antigens reflected in the work by de Haan *et al.*,^[35] the HA epitope was only incorporated C-terminally in SAGEs. However, SAGES were functionalized with TT and OVA both N- and C-terminally to allow for comparison of the effects of antigen positioning on downstream immune responses. The *in vitro* experiments with TT-functionalized SAGEs suggested that N-terminal functionalization decreased the uptake of SAGE, leading to a diminished ability to stimulate CD4⁺ T cell proliferation. By contrast, SAGES functionalized N-terminally with OVA stimulated a stronger CD4⁺ T cell proliferative response, but weaker antibody response compared to SAGES functionalized C-terminally with OVA. Whilst OVA-functionalized SAGE uptake by APCs has not been explored in as much detail as with TT functionality, these results suggest that N-terminal OVA does not affect

uptake levels in the same way that *N*-terminal TT does, as measured by downstream immune responses. We know from biophysical characterization that OVA functionality leads to the formation of larger particles and has a potentially destabilizing effect on component trimerization, and so it would be of interest to further probe the mechanism of internalization. Whether functionalization affects particle recognition and cellular uptake due to surface charge, differences in particle size or aggregation remains to be identified.

The *de novo* designed SAGE system provides an adaptable and predictable modular system that has easily accessible and interchangeable component parts. These components can be accessed synthetically or recombinantly, are not susceptible to problems associated with the cold chain and can be modified to successfully display antigens. The modularity of SAGEs means there is future potential for optimization in terms of charge, shape and size to drive the ideal antigen-specific response. In addition, the display of antigenic components can take the form of peptides or proteins,^[31a] whether linear, conformational or conjugated, to best promote the uptake, delivery and presentation of viral or bacterial antigens to the immune system. To date we have demonstrated that SAGE particles can act as successful scaffolds for the presentation of immunogenic peptide components, whilst maintaining their ability to self-assemble. We now seek to explore whether SAGEs can be used as a novel delivery system to drive further antigen-specific responses, and whether functionalizing with whole proteins helps to strengthen these responses. Finally, whether with continued peptide functionality or with whole proteins, the next important step will be to use SAGEs as a scaffold to effectively protect against an infection challenge.

4. Experimental Section

Solid-phase peptide synthesis (SPPS): Peptides were synthesized using a Liberty Blue microwave peptide synthesizer (CEM, Mathews, USA) on a 0.1 mmol scale, using 9-fluorenylmethoxycarbonyl (Fmoc) chemistry. Coupling was performed using *N,N'*-diisopropylcarbodiimide (DIC, 1 M in *N,N*-Dimethylformamide (DMF)) and 6-chloro-1-

hydroxybenzotriazole (CI-HOBT, 0.5 M in DMF), with morpholine (20 % in DMF) for deprotection. In all instances deprotection conditions were two treatments of 80 °C with 45 W for 300 s, with DMF washing in between. For Cys and His residues coupling conditions were 25 °C with 0 W for 120 s, followed by 50 °C with 25 W for 480 s. For Arg residues coupling conditions were 25 °C with 0 W for 2700 s, followed by 75 °C with 30 W for 120 s. For all other residues coupling conditions were 80 °C with 25 W for 300 s.

SAGE assembly: Hub variants were dissolved at the desired concentration, in the desired buffer, and left for 10 min before mixing. If assembling with more than one variant, for example the two HubB variants for ^{FITC}SAGE, the two were mixed and left for 10 min before introducing the partner hub component. Mixed hubs were allowed to assemble for 1 h before conducting characterization and experiments.

Circular dichroism (CD) spectroscopy: CD spectra were obtained using a JASCO J-810 or J-815 spectropolarimeter fitted with a Peltier temperature controller. Solutions were prepared (50 μM) in PBS (pH 7.4) and examined in a 1 mm quartz cuvette. Thermal denaturation experiments were performed by increasing the temperature from 5 °C to 90 °C at a rate of 40 °C h⁻¹. Spectra were measured at 5 °C intervals and the CD at 222 nm recorded at 1 °C intervals (1 nm intervals, 1 nm bandwidth, 16 s response time). Raw data (mdeg) were normalized for peptide concentration, pathlength and the number of amide bonds to give mean residue ellipticity (MRE, deg cm² dmol⁻¹ res⁻¹). Melting temperatures were obtained from the intercept of the x axis in a second derivative plot of MRE at 222 nm against temperature.

Scanning electron microscopy (SEM): Hubs were prepared in PBS (50 μM, pH 7.4) and mixed in a 1:1 ratio, allowing for SAGE assembly over 1 h (final total peptide concentration of 50 μM). Assembled SAGE (5 μl) was then deposited onto a carbon-coated stub and left overnight to air-dry, before sputter coating with gold/palladium (Emitech K575X, 30 s at 40 mA) to deposit a layer approximately 5 nm thick. Images were obtained using an FEI (Oregon, USA) Quanta 400 instrument.

AST assay: For the toxicity study, AST was evaluated in whole blood samples tested with a colorimetric method using a Konelab Prime 60i (Thermo Fisher).

Cellular uptake of fluorescent SAGE: Differentiated MDMs and MDDCs were seeded at equal densities of 5×10^5 per well in a 24 well plate, cells were washed with PBS prior to the addition of fluorescein isothiocyanate (FITC, $10 \mu\text{M}$ final concentration) functionalized particles ($^{\text{FITC}}$ SAGE) or left untreated for 0, 30, 90, 120 and 240 min. Cells were harvested on ice, manually detached and divided into two samples, trypan blue added to one sample (0.1% v/v final concentration) 15 min prior to flow cytometric acquisition in order to quench external fluorescence. Flow cytometry was performed using a LSRFortessa X-20 (BD Biosciences, San Diego, US). Analysis of unquenched versus quenched samples was performed using FlowJo software (BD Biosciences) and uptake of SAGE measured as Geomean fluorescence.

Cell proliferation assays: For TT-functionalized SAGE experiments, healthy donors aged 18-55 were recruited to the study and peripheral blood was obtained from these individuals. The study was approved by the local research ethics committee as part of the University of Bristol Immunity and Infection Research Tissue Bank (NHS REC 08/H0106/132; Licence no. 12248) and informed written consent was obtained from the donors in each case.

Human PBMC or murine splenocytes were grown in 24-well flat-bottomed plates (Corning, UK) in the presence of SAGE (2, 7.5 or $15 \mu\text{M}$), PHA ($10 \mu\text{g ml}^{-1}$; Sigma) or media only and were placed at 37°C , 5% CO_2 in a humidified environment for up to 10 days. Between days 3-10 of culture, triplicate samples ($100 \mu\text{l}$) from the resuspended cell cultures were plated into 96-well round bottomed plates (Corning, UK). Cultures were pulsed with $0.4 \mu\text{Ci}$ [^3H]- thymidine (Perkin Elmer, UK) overnight before harvesting using a 96-well harvester (Tomtec, USA) and assessment of [^3H]-thymidine incorporation using a Wallac Trilux 1450 β -scintillation counter (Perkin Elmer, UK). Proliferation was calculated as mean corrected counts per minute (CPM) for each triplicate. SAGE at 2, 7.5 and $15 \mu\text{M}$ is the equivalent of 12, 45 and $90 \mu\text{g ml}^{-1}$ total peptide respectively.

Immunization with OVA-functionalized SAGE: BALB/c mice (Jackson Laboratory, Charles River UK Limited) were used, where female mice were housed under specific pathogen free conditions in the University of Bristol Animal Services Unit and used at 12-16 weeks of age. All experiments were conducted in compliance with UK Home Office regulations.

Mice were immunized subcutaneously. On termination spleens were excised from animals and sieved through a series of cell strainers (40 μm ; BD Biosciences) to generate a single-cell suspension of murine splenocytes for *ex vivo* proliferation assays. After harvesting by centrifugation, the splenocytes were reconstituted in X-vivo 15 media (Lonza, Slough, UK) at 1×10^6 cells ml^{-1} and stimulated with either SAGE or OVA peptide. Antibody titers against SAGE and OVA were evaluated using end point titre enzyme-linked immunosorbent assay (EPT ELISA), and cell proliferation assays carried out as in *in vitro* experiments.

Labelling CL4 CD8⁺ T cells with CellTraceTM Violet (CTV): Proliferative assays were performed by labelling CL4 CD8⁺ cells with cell replication tracking CTV (Thermo Fisher). Enriched CL4 CD8⁺ cells were resuspended (4×10^6 cells ml^{-1} in PBS), then CTV ($1 \mu\text{l ml}^{-1}$) was added and incubated in the dark (20 min at 37 °C). The labelling was quenched with CM and cells left to settle (30 min at room temperature) before being resuspended in CM for *in vitro* cultures (2×10^6 cells ml^{-1}), or PBS for *in vivo* experiments ($3-5 \times 10^6$ cells ml^{-1} , 100 μl per mouse).

Adoptive Transfer of CL4 CD8⁺ T cells and SAGE-HA immunization in vivo: 6- to 8-week old Thy1.1^{+/+} CL4^{+/-} BALB/c TcR transgenic mice (recognising the hemagglutinin₅₁₈₋₅₂₆ epitope; bred in a pathogen-free environment at the University of Bristol Animal Services Unit) and Thy1.2^{+/+} BALB/c mice (Charles River UK Limited) were used. All experiments were conducted in accordance with current UK Home Office regulations.

CL4 CD8⁺ T cells labelled with CTV were resuspended in PBS (50 % CTV-CL4 cells and 50 % PBS). BALB/c mice were injected intravenously (i.v.) with CTV-CL4 cells ($3-5 \times 10^6$ cells, 100 μl i.v. per mouse), HA peptide (100 μl at 2 μM subcutaneously in dorsal neck scruff) or SAGE-HA (100 μl at 2 μM subcutaneously in dorsal neck scruff). 100 μl at 2 μM gives a

188 ng dose of HA epitope. Mice were assigned treatments in a manner designed to eliminate batch effects. After 3 days spleens were extracted from the mice, processed and enriched for CL4 cells, then stained for viability and cell surface markers.

Statistical analysis: Statistical analyses and graphical presentation were performed using GraphPad Prism 5 software. Significance of MDDC uptake of TT-functionalized SAGEs was determined by a 2 way ANOVA test (n = 6 donors). Significance of proliferative response to TT-functionalized SAGEs was determined by a Mann-Whitney test (n = 14 donors). Significance of immunisation with OVA-functionalized SAGEs was determined by a Mann-Whitney test (n = 6 donors). Significance of proliferative response to immunization with SAGE-HA was determined using a Welch's t test after an arcsine square root transformation of the data. Asterisks indicate significant differences (* P < 0.05, ** P < 0.01, *** P < 0.001).

Supporting Information

Supporting Information is available from the Wiley Online Library or from the author.

Acknowledgements

This work was supported by grants from the BBSRC (BB/L01386X/1) to Derek N. Woolfson. Caroline Morris is supported by BrisSynBio, a BBSRC/EPSRC Synthetic Biology Research Centre. Derek N. Woolfson holds a Royal Society Wolfson Research Merit Award (WM140008). Peptides were synthesized using the BrisSynBio CEM Liberty Blue peptide synthesizer (BB/L01386X/1). Peptides were analyzed and characterized by the EPSRC-funded Bruker Ultraflex MALDI TOF/TOF instrument (EP/K03927X/1), at the University of Bristol School of Chemistry Mass Spectrometry Facility, and the microscopy equipment of the Wolfson Bioimaging Facility (funded by the Medical Research Council and Wolfson Foundation). We would also like to thank the Flow Cytometry Facility at the University of Bristol Faculty of Biomedical Sciences for use of their instruments. We thank Dr. Joseph L. Beesley for providing ^{FITC}CC-Tri3 and ^{FITC}HubB, Dr. Guto G.

Rhys for assistance with AUC experiments, Dr. Alan Hedges for assistance with statistical analysis, Dr. Grace L. Edmunds for assistance with *in vivo* injection and spleen extraction, and all staff at the University of Bristol Animal Services Unit. Caroline Morris and Sarah J. Glennie contributed equally to the production of experimental results.

Received: ((will be filled in by the editorial staff))

Revised: ((will be filled in by the editorial staff))

Published online: ((will be filled in by the editorial staff))

Supporting Information

vSAGE: a modular vaccine platform combining self-assembled peptide cages and immunogenic peptides

*Caroline Morris, * Sarah J. Glennie, Hon S. Lam, Holly E. Baum, Dhinushi Kandage, Neil A. Williams, David J. Morgan, Derek N. Woolfson* and Andrew D. Davidson**

Materials and methods

Peptide synthesis materials: *N,N*-Dimethylformamide (DMF), 6-chloro-1-hydroxybenzotriazole (Cl-HOBT), diisopropylethylamine (DIPEA) and all L-amino acids were purchased from Cambridge Reagents Ltd (Hessle, UK). Resins were purchased from Merck Chemicals Ltd (Southampton, UK) and PCAS BioMatrix Inc (Quebec, Canada). Trifluoroacetic acid (TFA) and morpholine were purchased from Alfa Aesar (Massachusetts, USA). Aldrithiol-2 was purchased from Sigma-Aldrich (Missouri, USA). Diethyl ether was purchased from Honeywell (New Jersey, USA). Dichloromethane (DCM) and acetonitrile (MeCN) were purchased from VWR International (Pennsylvania, USA). *N,N'*-diisopropylcarbodiimide (DIC) and triisopropylsilane (TIPS) were purchased from Acros Organics (New Jersey, USA).

Peptide cleavage and purification: Peptides without added *N*-terminal functionality were acetylated on-resin by treating with acetic anhydride (3 eq), DIPEA (4.5 eq) and DMF (7 ml) for 20 min. Regardless of capping, the resin was washed with DCM (3 x 10 ml) and dried prior to peptide cleavage. Peptides were cleaved from the resin by treatment with a cleavage cocktail of TFA (95 %), TIPS (2.5 %) and H₂O (2.5 %) for 3 h with agitation. After filtering the suspended resin and evaporating the TFA, the peptide was precipitated in cold diethyl ether and pelleted by centrifuging. The peptide was dissolved in high-performance liquid chromatography (HPLC)

buffers (90 % MeCN with 0.1 % TFA in H₂O, and 0.1 % TFA in H₂O) and lyophilized. Successful syntheses were determined by matrix assisted laser desorption/ionization time-of-flight mass spectrometry (MALDI-TOF MS; Bruker ultrafleXtreme, USA), using α -cyano-4-hydroxycinnamic acid (CHCA) matrix (10 mg ml⁻¹ in H₂O:MeCN:TFA 50:50:0.1) and generally ion positive reflector mode, and then centrifuged (20 °C at 3000 rpm for 10 min) prior to purification to pellet insoluble material. Purification was achieved by reversed-phase (RP)-HPLC using a JASCO (Oklahoma, USA) chromatography system with either a preparative (Grace Vydac 218TP 5 μ C18, 300 Å, 150 x 4.6 mm) or semi-preparative (Phenomenex Luna 5 μ C18, 100 Å, 150 x 10 mm) column, eluting with linear gradients and a flow rate of 8 ml min⁻¹ or 3 ml min⁻¹ respectively. Buffer A = 0.1 % TFA in H₂O, buffer B = 0.1 % TFA in 90 % MeCN. Fractions were again analysed by MALDI-TOF MS, and their purity assessed by RP-HPLC using an analytical (Phenomenex Kinetex 5 μ C18, 100 Å, 100 x 4.6 mm) column before lyophilising.

Disulfide bond formation: Activation of Cys residues was achieved by a 30 min treatment of peptide (1 mg ml⁻¹ in H₂O, 10 mg scale) with aldrithiol-2 (10 eq in methanol, 1 ml/10 ml dissolved peptide) followed by extraction of any unreacted aldrithiol-2 with Et₂O (3 x 20 ml washing). The aqueous portion was then freeze-dried before analysing and purifying as in the initial work up. Formation of hubs by disulfide formation was achieved by mixing this activated peptide with either CC-Di-A or CC-Di-B for 1 h in phosphate buffered saline (PBS; NaCl (137 mM), KCl (2.7 mM), and phosphate buffer (10 mM)) at pH 7.4. Successful hub assembly was confirmed by MALDI-TOF mass spectrometry, and further purified as before.

Determining peptide concentration: Peptide concentrations were determined by UV absorption at 280 nm (ϵ_{280} Trp = 5690 mol⁻¹ cm⁻¹; ϵ_{280} Tyr = 1280 mol⁻¹ cm⁻¹) using a Thermo Scientific NanoDrop 2000 spectrophotometer. Concentrations of samples not containing a chromophore used a literature protocol^[41] to determine the absorbance at 214 nm (ϵ_{214} OVA = 26825 mol⁻¹ cm⁻¹).

Dynamic light scattering (DLS): The hydrodynamic diameter of hubs and assembled SAGEs were determined using a Malvern (Malvern, UK) Zetasizer Nanoseries instrument. Samples were prepared at 10 μM in PBS (pH 7.4). Data were collected over 10 min (10 repeat analyses of 10 x 6 s) at 20 °C and analysed using the associated DTS Nano Particle sizing software.

Analytical ultracentrifugation (AUC) sedimentation velocity experiments: Sedimentation velocity experiments were carried out using a Beckman Coulter Optima XL-A analytical ultracentrifuge with an An-60 Ti rotor, spinning at 60,000 rpm at 20 °C. A total of 120 absorbance scans were collected at 5 min intervals at an appropriate wavelength monitoring the peptide backbone for each sample, over a radial range of 5.8 to 7.3 cm. Peptides were prepared at 50 μM in PBS (pH 7.4). Data were fitted to a continuous $c(s)$ distribution at 95 % confidence using Sedfit^[42]. The density of the buffer was calculated using Sednterp (<http://rasmb.org/sednterp/>), and the partial specific volume of each trimer peptide was calculated using Sedfit: CC-Tri3 (0.7622 ml g⁻¹); TT-CC-Tri3 (0.7625 ml g⁻¹); CC-Tri3- TT (0.7625 ml g⁻¹); TT-CC-Tri3-TT (0.7626 ml g⁻¹); OVA-CC-Tri3 (0.7329 ml g⁻¹); CC-Tri3-OVA (0.7329 ml g⁻¹); CC-Tri3-HA (0.74933 ml g⁻¹).

Human peripheral blood mononuclear cells: Human peripheral blood mononuclear cells (PBMCs) were isolated from the blood of healthy donors by centrifugation at 700 g for 20 min on Histopaque density-gradient medium (Sigma). PBMCs were harvested, washed in Hanks' balanced salt solution (Invitrogen) and resuspended in complete RPMI (RPMI-1640 with penicillin (100 U ml⁻¹), streptomycin (0.1 mg ml⁻¹), L-glutamine (4 mM) and HEPES buffer (10 mM)). PBMCs were counted using trypan blue (0.4 % wt/vol; Sigma), reconstituted in complete RPMI at 1×10^6 cells ml⁻¹ with heat-inactivated human AB-serum (10 % vol/vol; Sigma), and incubated at 37 °C in CO₂ (5 %).

To produce monocyte-derived dendritic cells (MDDCs) and macrophages (MDMs), monocytes were first isolated from the PBMCs by negative selection using a Macs Monocyte Isolation Kit II, following the manufacturer's guidelines (Miltenyi Biotec Ltd., Bisley, UK), with a final purity of >80 %. Monocytes were reconstituted in complete RPMI and seeded at

1×10^6 cells ml^{-1} in recombinant human GM-CSF (rhGM-CSF, final concentration of 1000 U ml^{-1} ; R&D Systems, Abingdon, UK) and rhIL-4 (500 U ml^{-1}) for differentiation into MDDCs or rhGM-CSF (50 U ml^{-1} ; Miltenyi Biotec) and rhm-CSF (50 ng ml^{-1} ; Miltenyi Biotec) for differentiation into MDMs. Cells were incubated at $37 \text{ }^\circ\text{C}$ in CO_2 (5 %) for 5 days.

Phagocytic phenotyping and cytokine analysis with MDDCs and MDMs: After 5 days of differentiation, MDDCs and MDCs were incubated with media only, SAGE ($10 \text{ } \mu\text{M}$) or lipopolysaccharide (LPS, 100 ng ml^{-1} ; Sigma). Supernatants were removed from cell cultures after 48 h, centrifuged to remove any cell debris and stored at $-80 \text{ }^\circ\text{C}$ for subsequent analysis. Cells were harvested from the wells and expression of surface markers associated with cell activation and antigen presentation were assessed using the following antibodies: CD80–FITC, CD83-PE, CD25-PE-Cy5, CD86-PE-Cy7, HLA A,B,C-PB, HLA-DR-APC (Biolegend, London, UK). Flow cytometry was performed using a LSRFortessa X-20, 5000-10,000 cell events were collected and analysis performed using FlowJo software and fluorescence expressed as Geomean fluorescence. Cytokine production was assessed using a Multiplex human cytokine immunoassay kit (Millipore, UK) and analysed for the presence of TNF- α , IL-6, IL-1 β , IL-10, IL-12p70 and IL-1 α according to the manufacturer's instructions. Samples were analysed using a Luminex 200 machine (Luminex B V, The Netherlands).

End point titre enzyme-linked immunosorbent assay (EPT ELISA): Antibody titres against SAGE or OVA peptide were evaluated using EPT ELISA. Blood from human donors, or from BALB/c mice upon termination, was collected and centrifuged ($3,000 \text{ g}$ for 10 min). After separation, serum was extracted and stored at $-20 \text{ }^\circ\text{C}$ for future analysis. Nunc Maxisorp 96 well plates (Sigma) were coated with capture antigen by overnight incubation at $4 \text{ }^\circ\text{C}$ with either SAGE ($7.5 \text{ } \mu\text{M}$) or OVA peptide ($10 \text{ } \mu\text{g ml}^{-1}$) in PBS (pH 7.4). Plates were washed twice with PBS containing Tween (0.1 % v/v, PBS-T) before blocking with bovine serum albumin (BSA) in PBS (1% BSA-PBS; Sigma) for 1 h at $37 \text{ }^\circ\text{C}$. The blocking reagent was removed and the plates washed twice with PBS-T before the adding serum at an initial dilution of 1 in 10 and then performing two-

fold dilutions across the plate. After 1 h incubation at room temperature, the plates were washed four times with PBS-T, followed by the addition of a goat anti-human or anti-mouse IgG:HRP (Serotec, Kidlington, UK) at a 1:2000 dilution in PBS-T and 1 h incubation at room temperature. Plates were then washed four times before adding citrate phosphate buffer supplemented with the substrate o-phenylenediamine dihydrochloride hydrogen peroxide (OPD, 0.4 mg ml⁻¹, 30 %; Sigma). The plates were left to develop at room temperature before being stopped by 1 M H₂SO₄. The optical density was read at 490 nm and data was acquired and analysed using SoftMax Pro software (California, USA).

Production of splenocytes from Clone-4 TcR transgenic (CL4) mice: Spleens were collected from CL4 TcR transgenic mice using sterile instruments and kept in RPMI. Spleens were sectioned, then pressed through cell strainers (40 µm; Corning). This process was repeated several times whilst washing with Complete Medium (CM: RPMI with L-glutamine (Thermo Fisher) supplemented with foetal bovine serum (10 %; Thermo Scientific), penicillin/streptomycin (50 U mL⁻¹; Thermo Fisher) and β-mercaptoethanol (5 x 10⁻¹⁰ M; Sigma-Aldrich)). Red blood cells were lysed using ACK lysing buffer (1 ml per spleen; Thermo Fisher). Lysis was quenched after 3 min using CM (10 ml) then PBS (10 ml).

Magnetic-Activated Cell Sorting (MACS) for CD8⁺ T cells: Purified CL4 splenocytes were enriched for CD8⁺ T cells with MACS. The lymphocyte population was labelled with anti-CD8a MicroBeads (Miltenyi Biotec) in MACS buffer (PBS with BSA (5 %) and ethylenediaminetetraacetic acid (EDTA; 2 mM); 50 µl per spleen harvested) by incubating for 15 min at 4 °C. After incubation, labelled cells were separated using a MidiMACS Separator (Miltenyi Biotec), MidiMACS LS columns (Miltenyi Biotec) and MACS buffer. Unbound beads were removed by adding MACS buffer (10 ml) and centrifuging (5 min at 1400 rpm at 4 °C). Cells were resuspended in MACS buffer and run through an LS column in a MidiMACS Separator pre-washed with MACS buffer (6 ml). The eluent of the first flow-through was re-run to maximize

CD8⁺ cell yield. After removal from the MidiMACS separator, CD8⁺ cells were removed by plunging MACS buffer (6 ml) through the LS column.

CL4 CD8⁺ T cell gating: CTV-labelled clone-4 (Thy1.1⁺) CD8⁺ cells adoptively transferred into BALB/c mice (Thy1.2⁺) were selected for by gating for lymphocytes, single cells, live cells, CD8b⁺ and Thy1.1⁺. Density plots for CTV-labelled CL4 cells were generated by showing Thy1.1 (y-axis) against CTV (x-axis). Histograms were generated by showing cell count (y-axis) against CTV (x-axis).

CL4 CD8⁺ T cell viability staining: Zombie NIR[™] Fixable Viability Kit (BioLegend, USA) was used to reveal dead cell populations. Staining was carried out by incubating the cells (resuspended in 100 µl PBS) with the prepared dye (1 µl for 1 x 10⁶ cells) for 15 min at room temperature in the dark, before washing with FACS buffer (BSA (0.5 % (w/v); Sigma-Aldrich) in PBS).

CL4 CD8⁺ T cell surface staining: Cell surface staining was performed using fluorochrome-conjugated monoclonal antibodies (mAbs). DB Fc block[™] (BD Biosciences, UK) was used to prevent non-specific binding of mAbs to Fc receptors on T cells (incubation for 15 min at 4 °C). Cells were then spun down and resuspended. The optimum volume of the following mAbs required for staining was then added (incubated in the dark at 4 °C for 30 min): CD8β-PE-Cy7, Thy1.1-PerCP-Cy5.5 (Biolegend). Cells were then washed with FACS buffer to remove any unbound antibody. Labelled cells were resuspended in paraformaldehyde (PFA; 1 %) for flow cytometric analysis the following day. 5000-10,000 live CL4 cells were analyzed using LSR II flow cytometer (BD Biosciences).

Name	Sequence			MW (Da)				
	<i>g</i>	<i>a</i>	<i>b</i>					
CC-Tri3	Ac-G	EIAAIKK	EIAAIKC	EIAAIKQ	GYG-NH	2630.11		
CC-Di-A	Ac-G	EIAALEK	ENAALEC	EIAALEQ	GWV-NH	2786.08		
CC-Di-B	Ac-G	KIAALKK	KNAALKC	KIAALKQ	GYW-NH	2757.39		
^{Fmoc} CC-Tri3	FITC-GG	G	EIAAIKK	EIAAIKC	EIAAIKQ	GYG-NH	3062.54	
TT-CC-Tri3	H-IDKISDVSTIVPYIGPALNI	GG	G	EIAAIKKEIAAIKCEIAAIKQGYG	NH	4812.63		
CC-Tri3-TT	Ac-G	EIAAIKKEIAAIKCEIAAIKQGYG	GG	IDKISDVSTIVPYIGPALNI	-OH	4855.65		
TT-CC-Tri3-TT	H-IDKISDVSTIVPYIGPALNI	GG	G	EIAAIKKEIAAIKCEIAAIKQGYG	GG	IDKISDVSTIVPYIGPALNI	-OH	7038.16
OVA-CC-Tri3	H-ISQAVHAAHAEINEAGR	GG	ISQAVHAAHAEINEAGR	GG	G	EIAAIKKEIAAIKCEIAAIKQGYG	NH	6328.06
CC-Tri3-OVA	Ac-G	EIAAIKKEIAAIKCEIAAIKQGYG	GG	ISQAVHAAHAEINEAGR	GG	ISQAVHAAHAEINEAGR	-OH	6371.08
CC-Tri3-HA	Ac-G	EIAAIKKEIAAIKCEIAAIKQGYG	GG	AVGAGATAEEIYSTVASSL	-OH	4524.11		
TT	H-IDKISDVSTIVPYIGPALNI	-OH				2128.46		
OVA	H-ISQAVHAAHAEINEAGR	-OH				1773.90		
HA	H-AVGAGATAEEI YSTVASSL	-OH				1796.93		

Table S1: Details of synthesized peptides. Peptide name, sequence and molecular weight (MW; Da). Peptides synthesized by Fmoc-SPPS as described in the SI materials and methods. The termini were capped when the *de novo* sequence was terminal (*N*-terminal acetylation, *C*-terminal amidation). HA sequence in bold represents the influenza virus A/PR/8/34 (H1N1) hemagglutinin₅₁₈₋₅₂₆ epitope sequence.

Hub name	Homotrimer component	Heterodimer component	MW (Da)
HubA	CC-Tri3	CC-Di-A	5414.19
HubB	CC-Tri3	CC-Di-B	5385.50
^{FITC} HubB	^{FITC} CC-Tri3	CC-Di-B	5817.93
TT-HubA	TT-CC-Tri3	CC-Di-A	7596.71
TT-HubB	TT-CC-Tri3	CC-Di-B	7568.02
HubA-TT	CC-Tri3-TT	CC-Di-A	7639.68
HubB-TT	CC-Tri3-TT	CC-Di-B	7611.04
TT-HubA-TT	TT-CC-Tri3-TT	CC-Di-A	9822.24
TT-HubB-TT	TT-CC-Tri3-TT	CC-Di-B	9793.55
OVA-HubA	OVA-CC-Tri3	CC-Di-A	9112.14
OVA-HubB	OVA-CC-Tri3	CC-Di-B	9083.45
HubA-OVA	CC-Tri3-OVA	CC-Di-A	9155.16
HubB-OVA	CC-Tri3-OVA	CC-Di-B	9126.47
HubA-HA	CC-Tri3-HA	CC-Di-A	7308.19
HubB-HA	CC-Tri3-HA	CC-Di-B	7281.50

Table S2: Details of prepared hub building blocks. Name, component peptides and MW of hub building blocks. The hubs were assembled by formation of a disulfide bond, as described in SI Methods and Materials

SAGE name	HubA variant	HubB variant
Parent SAGE	HubA (50 %)	HubB (50 %)
^{FITC} SAGE	HubA (50 %)	HubB (45 %) + ^{FITC} HubB (5 %)
TT-SAGE	TT-HubA (50 %)	TT-HubB (50 %)
SAGE-TT	HubA-TT (50 %)	HubB-TT (50 %)
TT-SAGE-TT	TT-HubA-TT (50 %)	TT-HubB-TT (50 %)
TT- ^{FITC} SAGE	TT-HubA (50 %)	TT-HubB (45 %) + ^{FITC} HubB (5 %)
^{FITC} SAGE-TT	HubA-TT (50 %)	HubB-TT (45 %) + ^{FITC} HubB (5 %)
TT- ^{FITC} SAGE-TT	TT-HubA-TT (50 %)	TT-HubB-TT (45 %) + ^{FITC} HubB (5 %)
OVA-SAGE	OVA-HubA (50 %)	OVA-HubB (50 %)
SAGE-OVA	HubA-OVA (50 %)	HubB-OVA (50 %)
SAGE-HA	HubA-HA (50 %)	HubB-HA (50 %)

Table S3: Details of assembled SAGEs. Name and component hubs of assembled SAGE designs. Hub variants were separately dissolved in appropriate buffer and left for 10 min before mixing and leaving to assemble for 1 h.

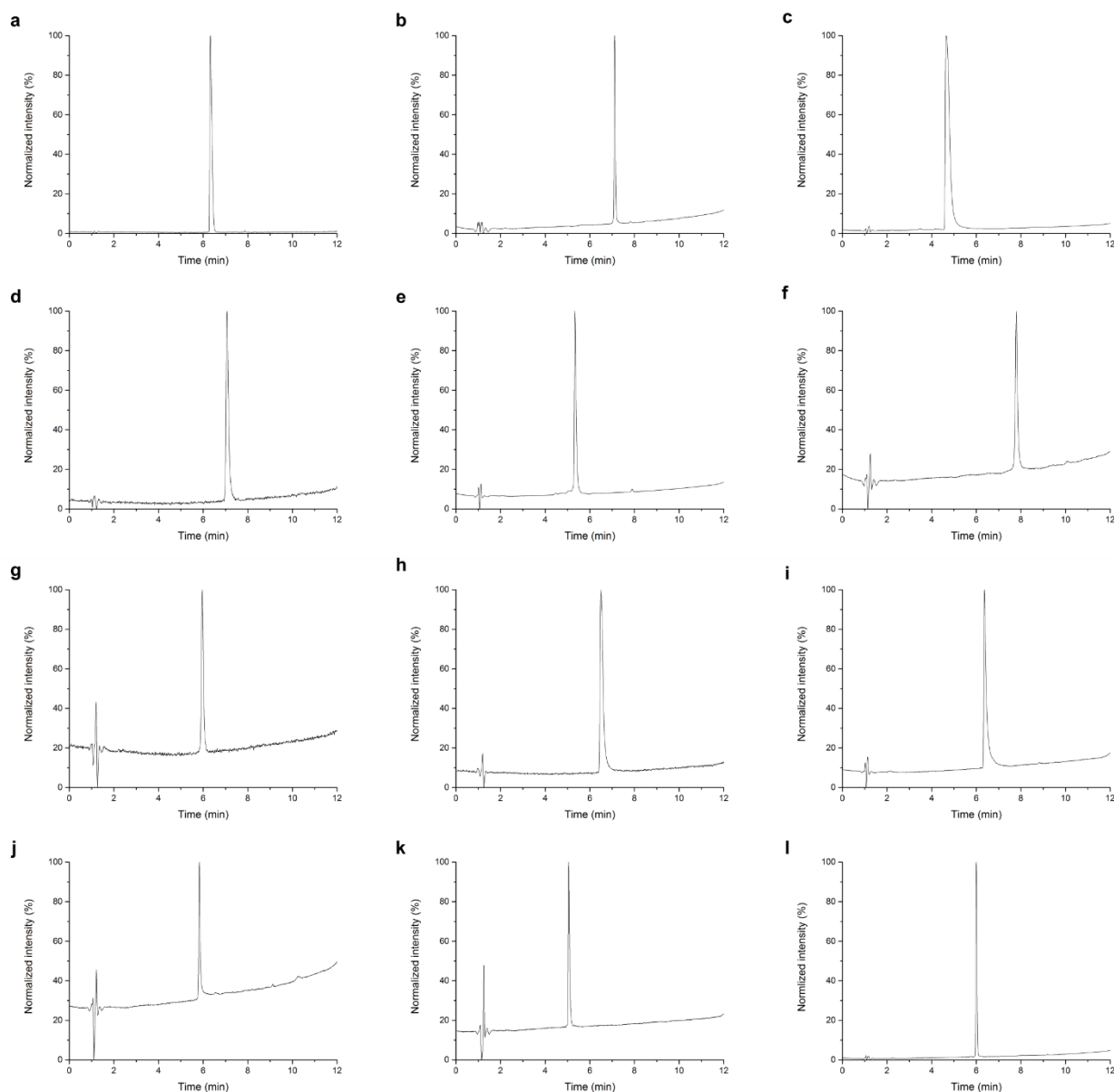


Figure S1: Analytical-HPLC for peptide components. **a** CC-Tri3 (20-80 % B in 9 min). **b** CC-Di-A (20-80 % B in 9 min). **c** CC-Di-B (20-80 % B in 9 min). **d** TT-CC-Tri3 (20-80 % B in 9 min). **e** CC-Tri3-TT (30-80 % B in 9 min). **f** TT-CC-Tri3-TT (20-80 % B in 9 min). **g** OVA-CC-Tri3 (20-80 % B in 9 min). **h** CC-Tri3-OVA (20-80 % B in 9 min). **i** CC-Tri3-HA (30-80 % B in 9 min). **j** TT (20-80 % B in 9 min). **k** OVA (10-60 % B in 9 min). **l** HA (10-80 % B in 9 min). Conditions: Buffer A = 0.1 % TFA in H₂O, buffer B = 0.1 % TFA in 90 % MeCN. Peptides dissolved in HPLC buffers and run on an analytical (Phenomenex Kinetex 5 μ C18, 100 \AA , 100 x 4.6 mm) column with a flow rate of 1 ml min⁻¹, monitoring at 280 nm (220 nm in **k**).

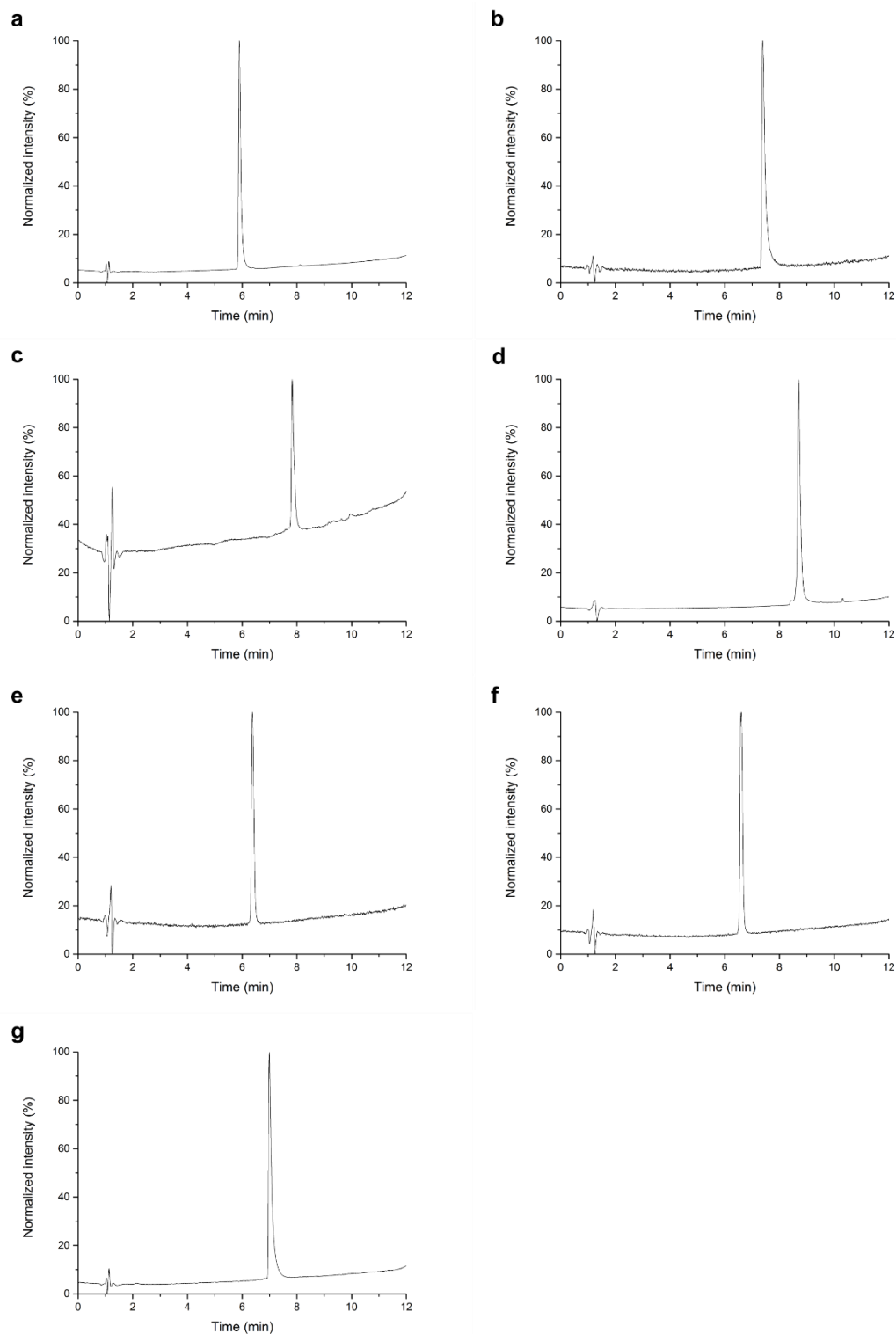


Figure S2: Analytical-HPLC for HubA variants. **a** HubA (20-80 % B in 9 min). **b** TT-HubA (20-80 % B in 9 min). **c** HubA-TT (20-80 % B in 9 min). **d** TT-HubA-TT (20-80 % B in 9 min). **e** OVA-HubA (20-80 % B in 9 min). **f** HubA-OVA (20-80 % B in 9 min). **g** HubA-HA (30-80 % B in 9 min). Conditions: Buffer A = 0.1 % TFA in H₂O, buffer B = 0.1 % TFA in 90 % MeCN. Peptides dissolved in HPLC buffers and run on an analytical (Phenomenex Kinetex 5 μ C18, 100 \AA , 100 x 4.6 mm) column with a flow rate of 1 ml min⁻¹, monitoring at 280 nm.

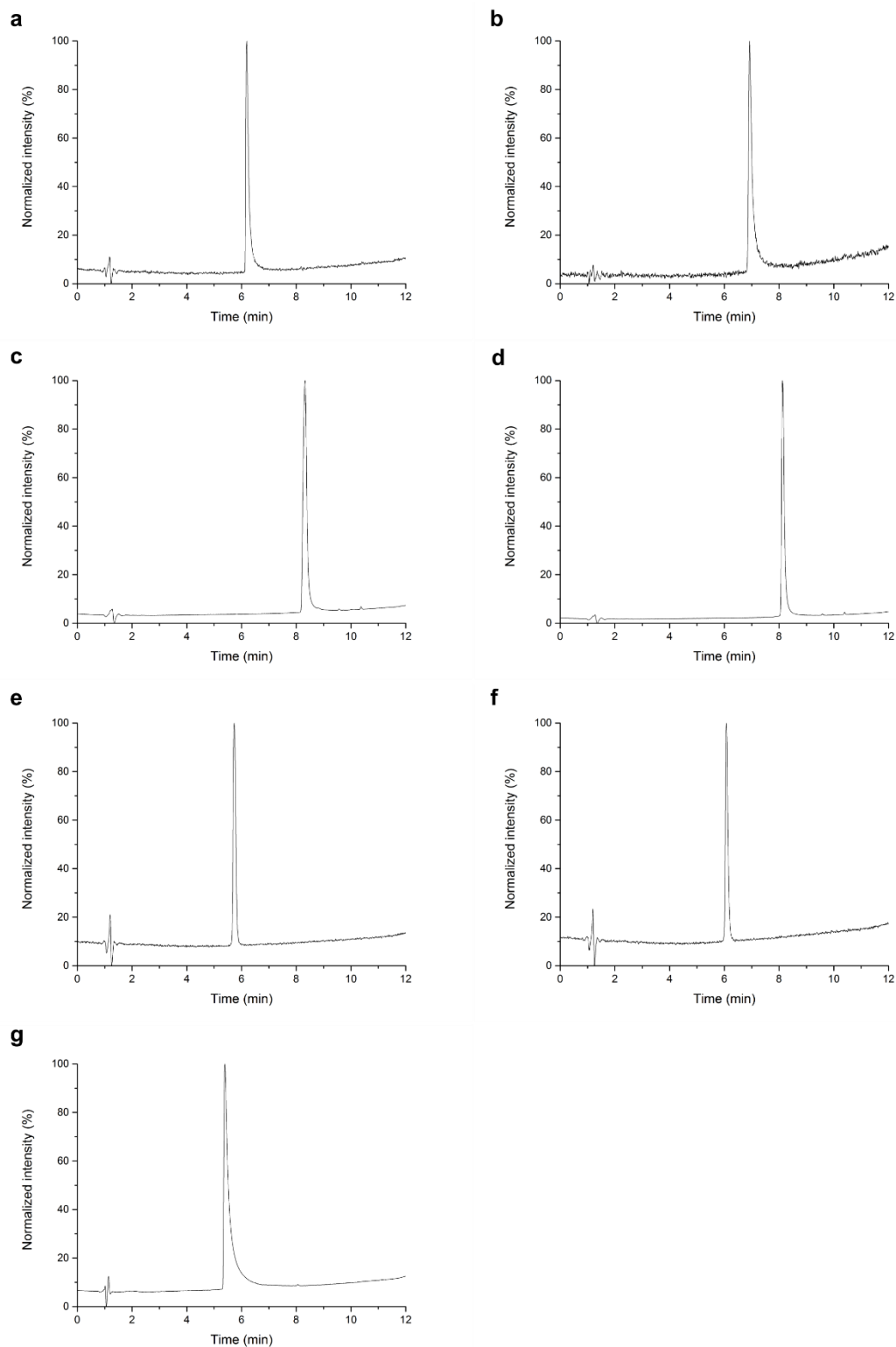


Figure S3: Analytical-HPLC for HubB variants. **a** HubB (20-80 % B in 9 min). **b** TT-HubB (20-80 % B in 9 min). **c** HubB-TT (20-80 % B in 9 min). **d** TT-HubB-TT (20-80 % B in 9 min). **e** OVA-HubB (20-80 % B in 9 min). **f** HubB-OVA (20-80 % B in 9 min). **g** HubB-HA (30-80 % B in 9 min). Conditions: Buffer A = 0.1 % TFA in H₂O, buffer B = 0.1 % TFA in 90 % MeCN. Peptides dissolved in HPLC buffers and run on an analytical (Phenomenex Kinetex 5 μ C18, 100 \AA , 100 x 4.6 mm) column with a flow rate of 1 ml min⁻¹, monitoring at 280 nm.

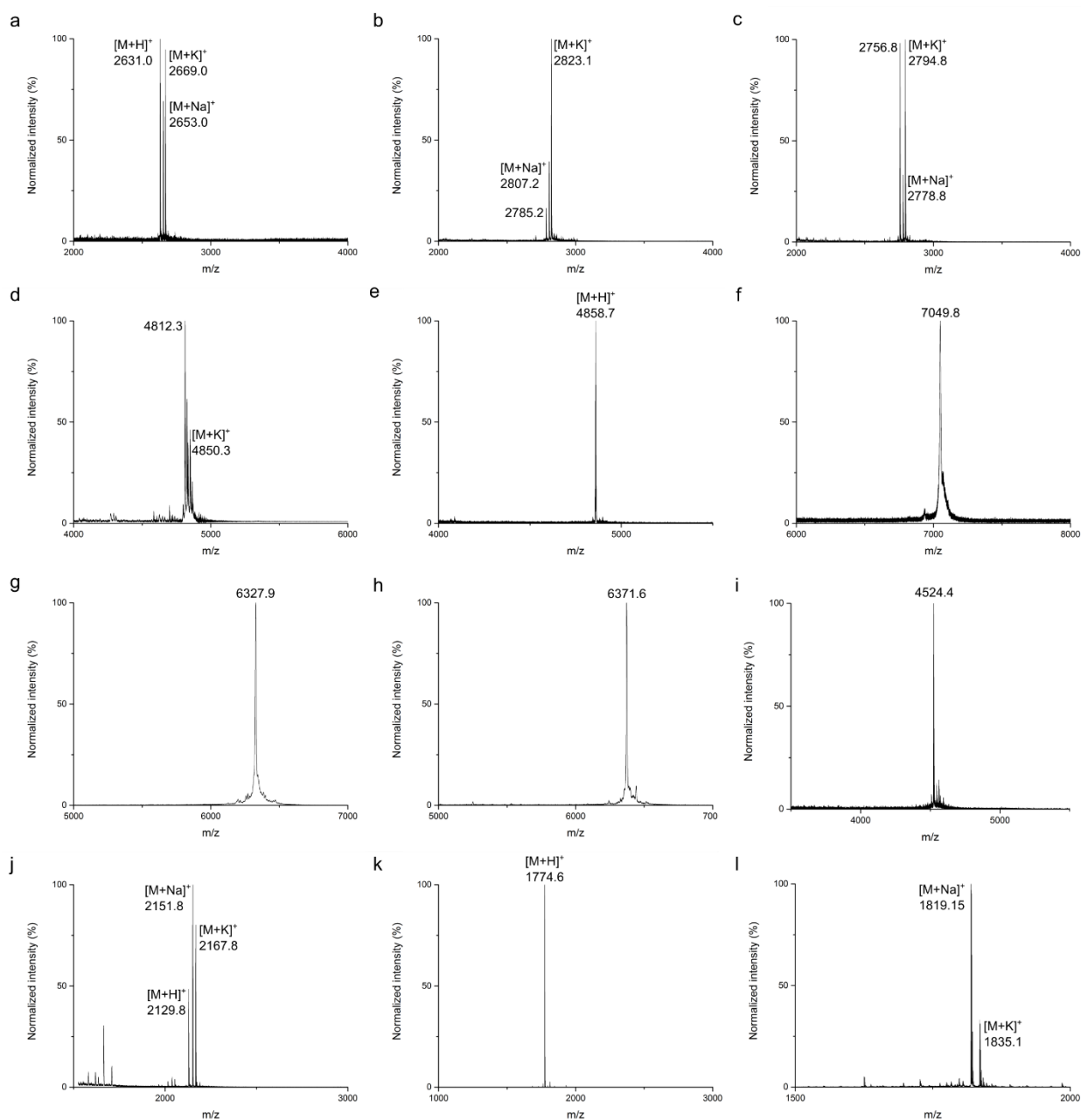


Fig S4: MALDI-TOF MS for peptide components. a CC-Tri3 (expected = 2630.1 Da). **b** CC-Di-A (expected = 2786.1 Da). **c** CC-Di-B (expected = 2757.4 Da). **d** TT-CC-Tri3 (expected = 4812.6 Da). **e** CC-Tri3-TT (expected = 4855.7 Da). **f** TT-CC-Tri3-TT (expected = 7038.2 Da). **g** OVA-CC-Tri3 (expected = 6328.1 Da). **h** CC-Tri3-OVA (expected = 6371.1 Da). **i** CC-Tri3-HA (expected = 4524.1 Da). **j** TT (expected = 2128.5 Da). **k** OVA (expected = 1773.9 Da). **l** HA (expected = 1796.9 Da). Conditions: Peptides mixed with α -cyano-4-hydroxycinnamic acid (CHCA) matrix (10 mg ml⁻¹ in H₂O:MeCN:TFA 50:50:0.1) and detected with ion positive reflector or linear mode.

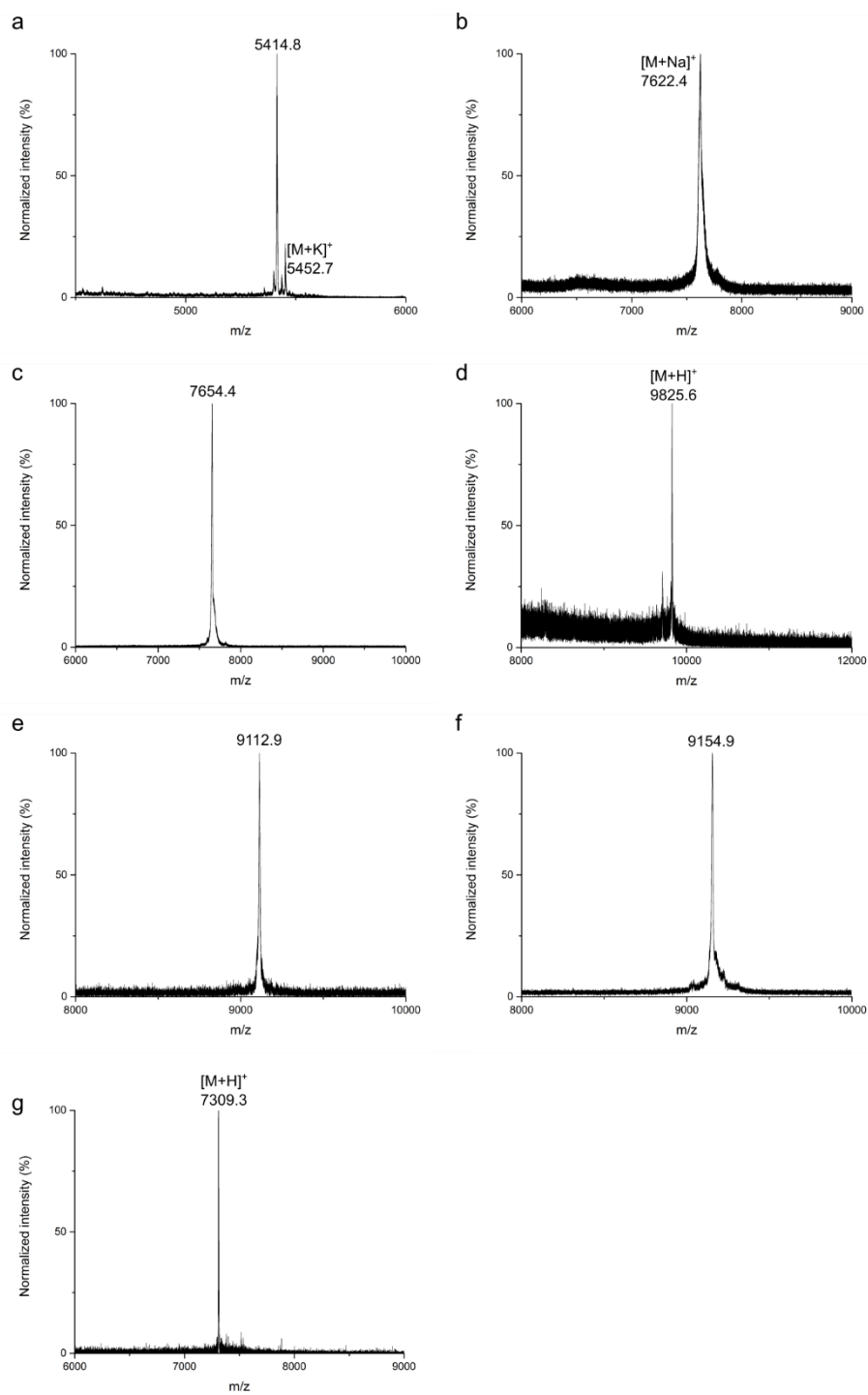


Fig S5: MALDI-TOF MS for HubA variants. **a** HubA (expected = 5414.2 Da). **b** TT-HubA (expected = 7596.7 Da). **c** HubA-TT (expected = 7639.7 Da). **d** TT-HubA-TT (expected = 9822.2 Da). **e** OVA-HubA (expected = 9112.1 Da). **f** HubA-OVA (expected = 9155.2 Da). **g** HubA-HA (expected = 7308.2 Da). Conditions: Peptides mixed with α -cyano-4-hydroxycinnamic acid (CHCA) matrix (10 mg ml⁻¹ in H₂O:MeCN:TFA 50:50:0.1) and detected with ion positive reflector or linear mode.

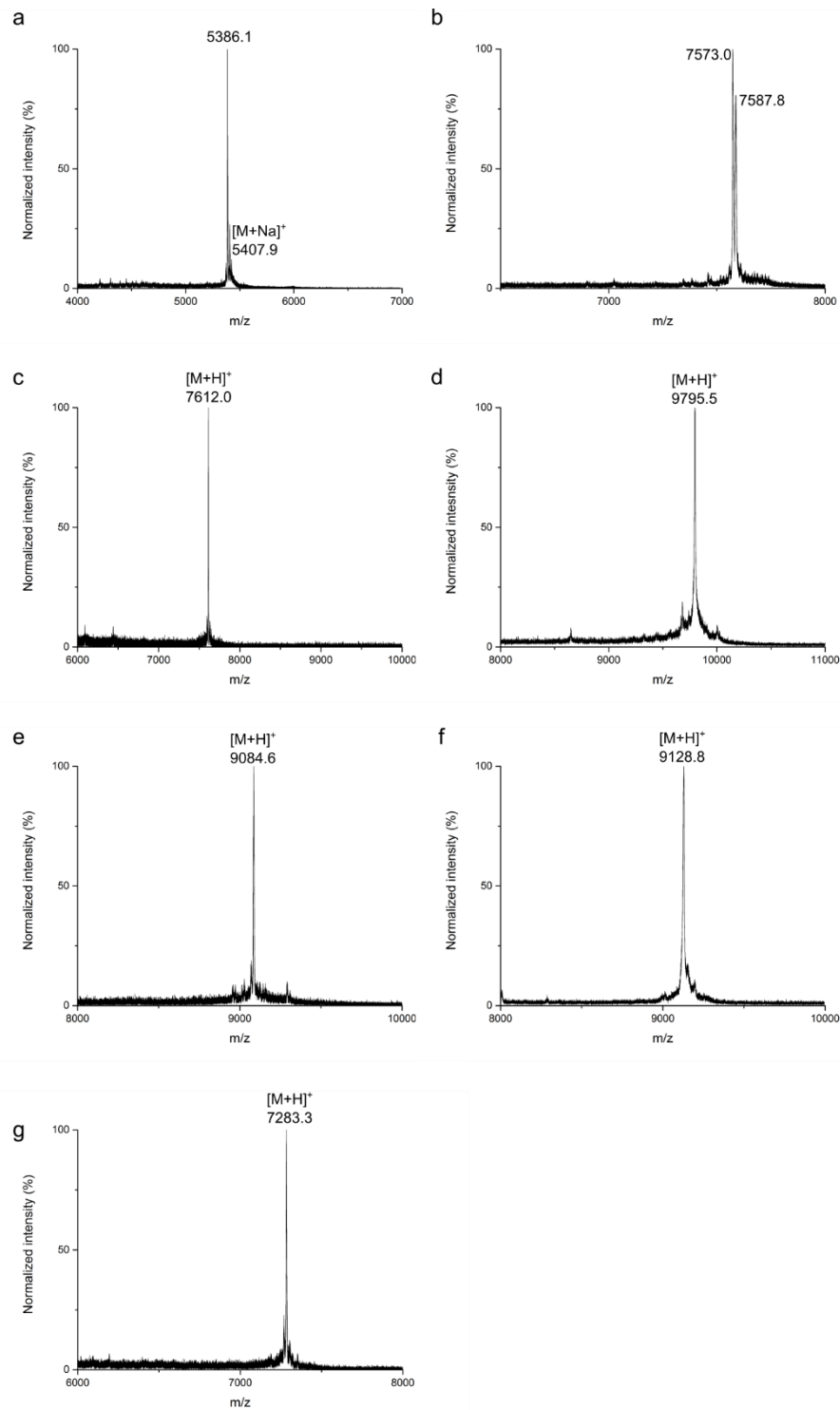


Fig S6: MALDI-TOF MS for HubB variants. **a** HubB (expected = 5385.5 Da). **b** TT-HubB (expected = 7568.0 Da). **c** HubB-TT (expected = 7611.0 Da). **d** TT-HubB-TT (expected = 9793.6 Da). **e** OVA-HubB (expected = 9083.5 Da). **f** HubB-OVA (expected = 9126.5 Da). **g** HubB-HA (expected = 7281.5 Da). Conditions: Peptides mixed with α -cyano-4-hydroxycinnamic acid (CHCA) matrix (10 mg ml^{-1} in $\text{H}_2\text{O}:\text{MeCN}:\text{TFA}$ 50:50:0.1) and detected with ion positive reflector or linear mode.

Peptide	T _M (°C)	MRE _{222nm} (deg cm ² dmol ⁻¹ res ⁻¹)	Fraction helix (%)	Normalized MRE _{222nm} (deg cm ² dmol ⁻¹ res ⁻¹)	Normalized fraction helix (%)
CC-Tri3	55	-29556.41	79.3	-29556.41	79.3
TT-CC-Tri3	61	-17646.45	45.0	-32469.46	81.9
CC-Tri3-TT	51	-12444.69	32.0	-22400.39	56.8
TT-CC-Tri3-TT	56	-9934.31	25.7	-27021.28	68.2
OVA-CC-Tri3	55	-13153.92	33.8	-32621.71	82.2
CC-Tri3-OVA	54	-10561.92	29.8	-26616.03	73.4
CC-Tri3-HA	53	-14011.11	35.9	-25780.44	69.3

Table S4: Circular dichroism (CD) data for each CC-Tri3 peptide synthesized. Midpoint of thermal unfolding (T_M) of functionalized trimer peptides relative to parent as determined by CD spectroscopy when ramping the temperature from 5-90 °C at a rate of 40 °Ch⁻¹; mean residue ellipticity (MRE) at 222 nm of each peptide at 5 °C; observed fraction helix as determined using:

$$Fraction\ helix\ (\%) = 100 \left(\frac{([\theta]_{222} - [\theta]_{coil})}{(-42,500(1 - (3/n)) - [\theta]_{coil})} \right)$$

Where $[\theta]_{coil} = 640 - 45T = 415 \text{ deg cm}^2 \text{ dmol}^{-1} \text{ res}^{-1}$ at 5 °C, and n is the number of peptide bonds (including N terminal acetylation). These calculations are repeated using MRE values normalized to the length of the parent trimer (25 residues) to assess any impact on the degree of the helical component.

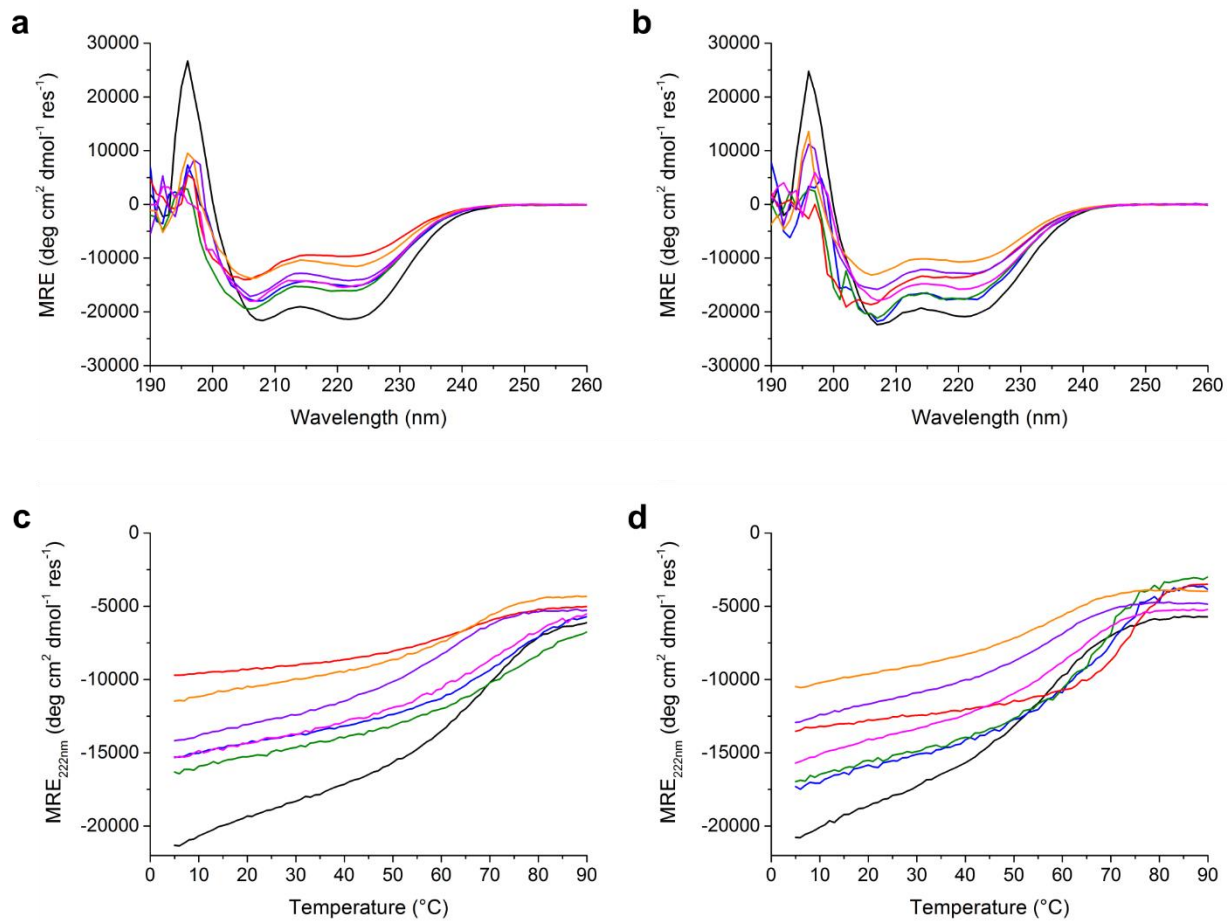


Fig S7: CD data for hub variants. **a** 5 °C wavelength scans of HubA variants. **b** 5 °C wavelength scans of HubB variants. **c** Thermal denaturation curves of HubA variants. **d** Thermal denaturation curves of HubB variants. **a-d** conditions: hubs at 50 μ M in PBS (pH 7.4). Comparison of parent hubs containing CC-Tri3 (black) with functionalized hubs containing TT-CC-Tri3 (blue), CC-Tri3-TT (green), TT-CC-Tri3-TT (red), OVA-CC-Tri3 (purple), CC-Tri3-OVA (orange) and CC-Tri3-HA (pink).

SAGE design	HubA variant	HubB variant
	T_M (°C)	T_M (°C)
Parent	69	57
TT-SAGE	72	68
SAGE-TT	73	67
TT-SAGE-TT	63	73
OVA-SAGE	59	56
SAGE-OVA	64	56
SAGE-HA	72	62

Table S5: Midpoint of thermal unfolding (T_M) for functionalized hubs in each SAGE design. T_M values of functionalized hub components when ramping the temperature from 5-90 °C at a rate of 40 °C h⁻¹. Hubs at 50 μM in PBS (pH 7.4).

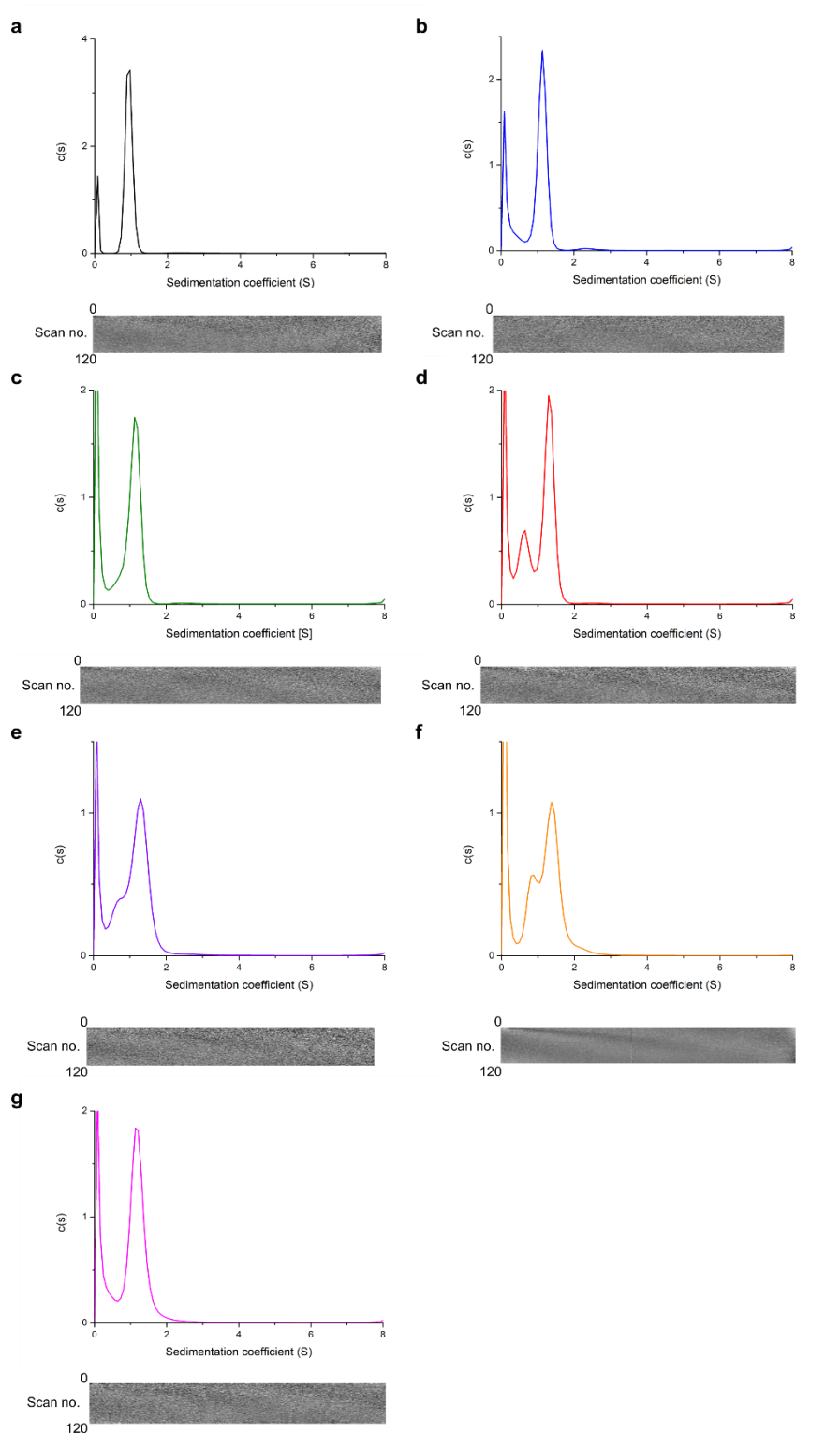


Fig S8: Analytical ultracentrifugation (AUC) data for each homotrimeric peptide. AUC SV data fits (top) and residuals (bottom) for functionalized trimer peptides. Continuous $c(s)$ distribution from sedimentation-velocity data at 60 k rpm, 20 °C. **a** CC-Tri3, giving 8.47 kDa (3.2 x monomer mass). **b** TT-CC-Tri3, giving 14.1 kDa (2.9 x monomer mass). **c** CC-Tri3-TT, giving 13.1 kDa (2.7 x monomer mass). **d** TT-CC-Tri3-TT, giving 20.3 kDa (2.9 x monomer mass) and 7.12 kDa (monomer). **e** OVA-CC-Tri3, giving 12.2 kDa (1.9 x monomer mass). **f** CC-Tri3-OVA, giving 22.1 kDa (3.5 x monomer mass) and 10.1 kDa (1.6 x monomer mass). **g** CC-Tri3-HA, giving 12.7 kDa (2.8 x monomer mass). Peptides at 50 μ M in PBS (pH 7.4).

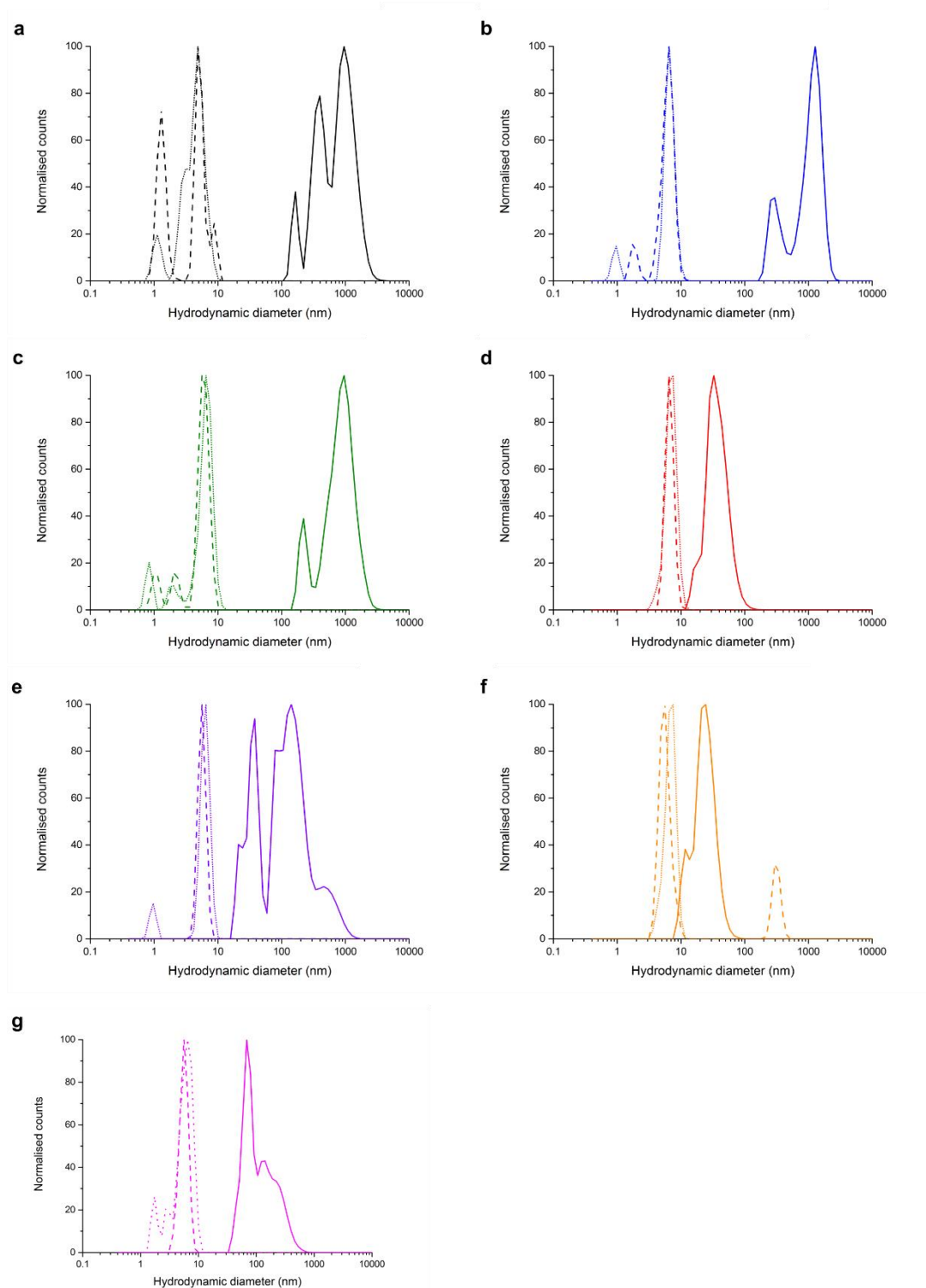


Figure S9: Dynamic light scattering (DLS) data for each SAGE design. Data were collected over 10 min (10 repeat analyses of 10 x 6 s) at 20 °C, allowing for plotting of hydrodynamic diameter against time. Hub components (HubA variant = dotted line, HubB variant = dashed line) and SAGE assembly (solid lines) were analysed. **a** parent SAGE. **b** TT-SAGE. **c** SAGE-TT. **d** TT-SAGE-TT. **e** OVA-SAGE. **f** SAGE-OVA. **g** SAGE-HA. Hubs were prepared at 10 μ M in PBS (pH 7.4).

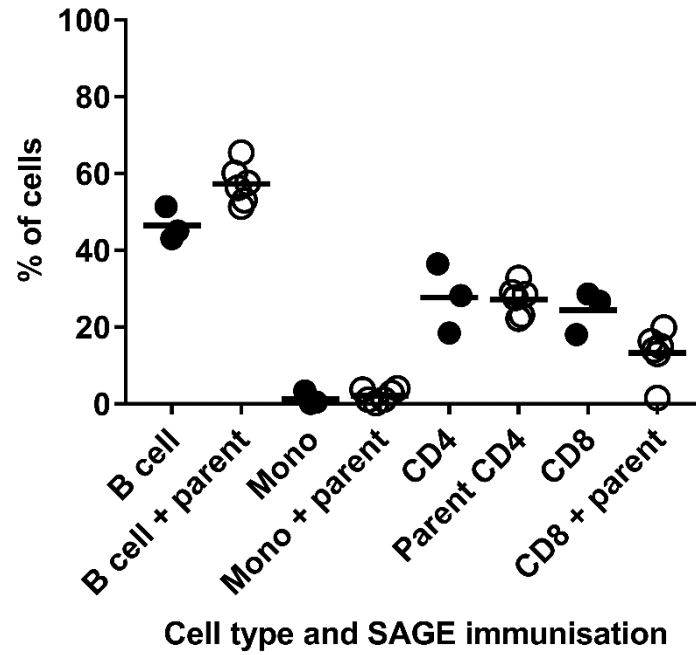
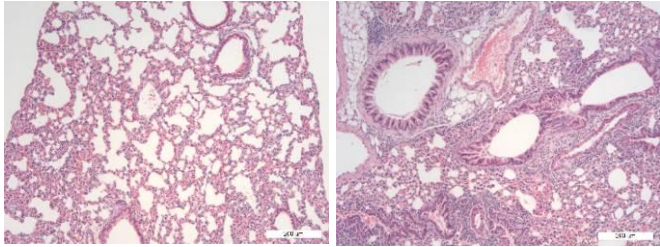
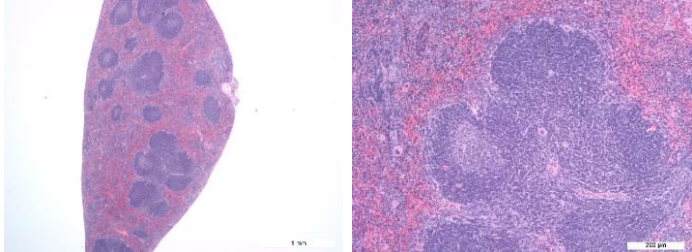
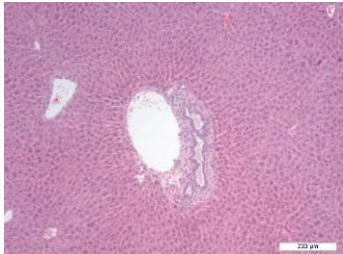
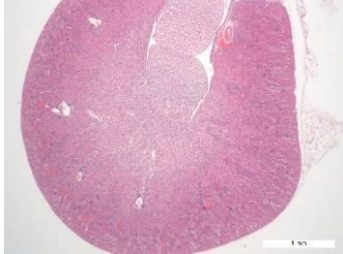
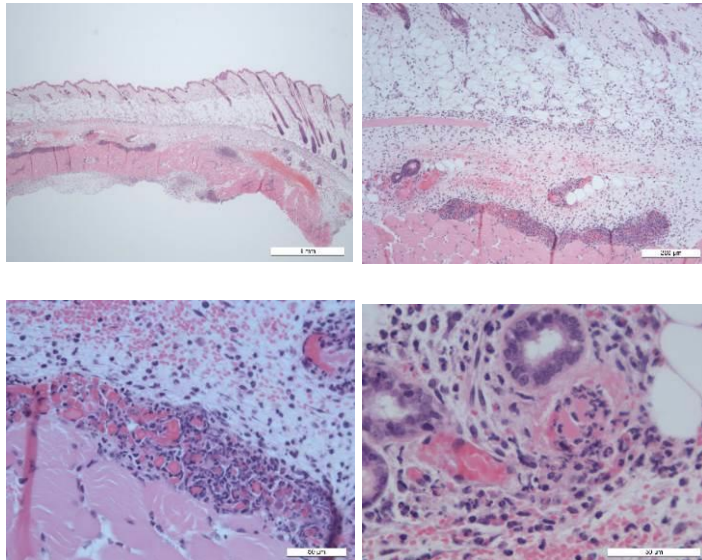


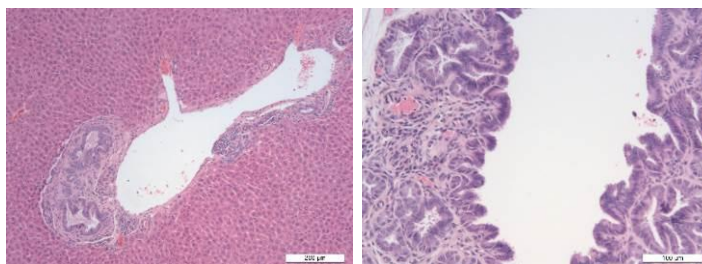
Figure S10: Representation of cell populations during *in vivo* toxicity assay. Populations of B cells, monocytes, CD4 and CD8 T cells in peripheral blood isolated from control animals immunized with PBS (pH 7.4) alone and those immunized with parent SAGE. BALB/c mice were immunized with four doses (350 μ g) of parent SAGE, each dose at an interval of 3 weeks (2 weeks for the final immunisation). Control group: n = 3 mice; test group: n = 6 mice.

Animal Number	Tissue	Comments
1.1	Lung	Five sections. Each shows multifocal mild to moderate interstitial pneumonia. One section shows a region of moderate peribronchiolar/arteriolar lymphoplasmacytic infiltration with some eosinophils.
		
	Spleen	Single section. Normal to active white pulp with secondary follicles. Haemopoietic activity in red pulp.
		
	Liver	Five sections. Histologically normal liver.
		
	Kidney	Two sections. Histologically normal kidney, including cortex and medulla.
		
	Injection site	One strip of skin including panniculus muscle, subcutis and deep muscle block. There is diffuse mild to moderate dermal to subcutaneous oedema and focal microhaemorrhage, with chiefly pyogranulomatous

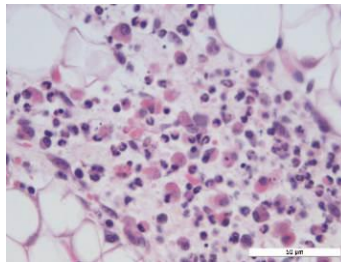
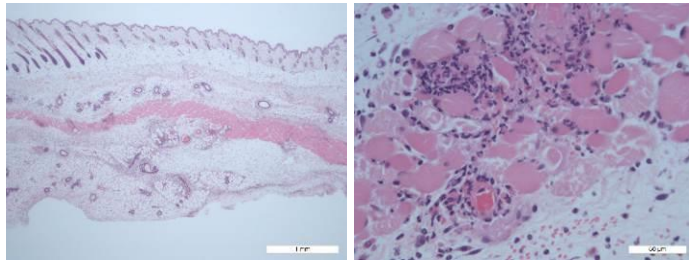
inflammation and some focal lymphoplasmacytic aggregates (a). There is thrombosis/vasculitis of some small vessels (d). Immediately above the deep muscle block is a plaque of brightly eosinophilic particulate material (adjuvant material?) enveloped by primarily pyogranulomatous inflammation (b and c).



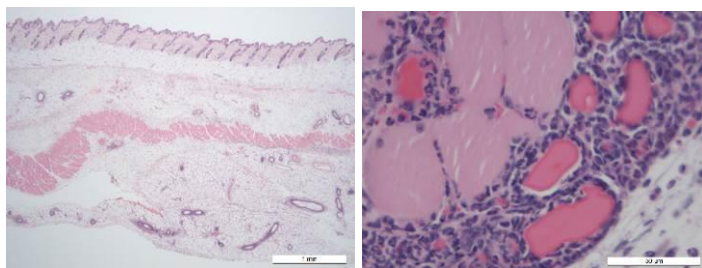
- | | | |
|-----|----------------|---|
| 1.2 | Lung | Five sections of lung with mild to moderate interstitial pneumonia as above. |
| | Spleen | Single section of normal/reactive spleen as above. |
| | Liver | Five sections of liver with normal microarchitecture. There is focal mild portal fibrosis and bile duct proliferation associated with mild lymphoplasmacytic inflammation. One section includes gall bladder which also shows mild inflammation. Diagnosis: mild cholecystitis. |
| | Kidney | Two sections of normal kidney including cortex and medulla. |
| | Injection site | Strip of skin with deep muscle block and underlying adipose tissue (a). Diffuse oedema, microhaemorrhage and inflammation (neutrophils and macrophages with prominent erythrophagocytosis) in all layers (c). |



Vasculitis and thrombosis multiple, with focal myonecrosis of muscle block (b). No eosinophilic material as noted in 1.1.



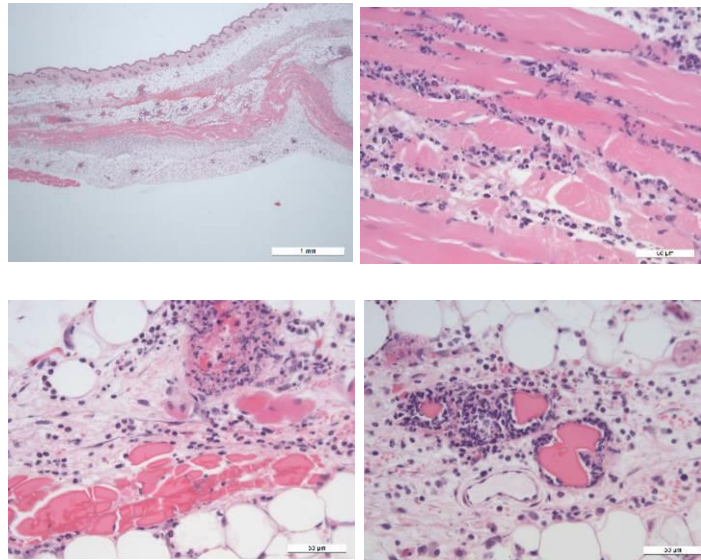
- | | | |
|-----|----------------|---|
| 1.3 | Lung | Five sections of lung with moderate interstitial pneumonia as described above. |
| | Spleen | One section of normal/reactive spleen as described above. |
| | Liver | Five sections of normal liver. |
| | Kidney | Two sections of normal kidney including cortex and medulla. |
| | Injection site | Strip of skin with similar range of changes to those described above, but slightly milder with fewer examples of vasculitis/thrombosis. Single small area at one margin includes angular eosinophilic material with surrounding inflammatory cells (b). |



- | | | |
|-----|--------|--|
| 1.4 | Lung | Five sections of lung with mild to moderate interstitial pneumonia as above. |
| | Spleen | Section of normal/reactive spleen. |
| | Liver | Five sections of normal liver. |

Kidney Two sections of normal kidney; cortex and medulla.

Injection site Strip of skin with changes as described above. Diffuse dermal to subcutaneous oedema, microhaemorrhage and inflammation. More prominent focal myositis and myonecrosis. A plaque of eosinophilic material within the subcutis with surrounding inflammation in part.



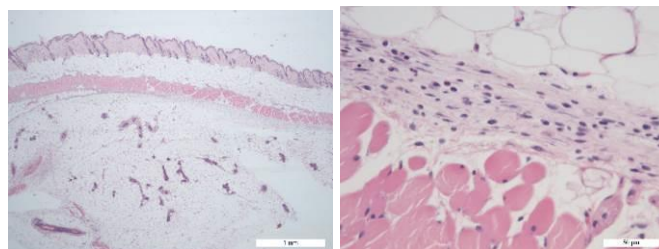
1.5 Lung Five sections of lung with moderate interstitial pneumonia as above.

Spleen Section of normal/reactive spleen. Also includes a small portion of normal exocrine pancreas.

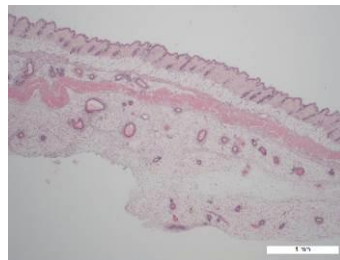
Liver Five sections of normal liver. Occasional small portal aggregates of mixed mononuclear and granulocytic cells regarded as incidental.

Kidney Two sections of normal kidney; cortex and medulla.

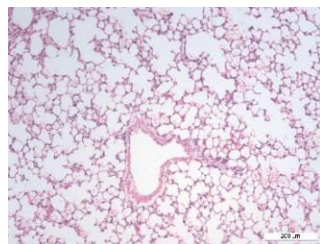
Injection site Strip of largely normal skin. The only change of note is the presence of a mild band of early fibroblastic proliferation and scattered inflammatory cells at the deep margin of the muscle block.



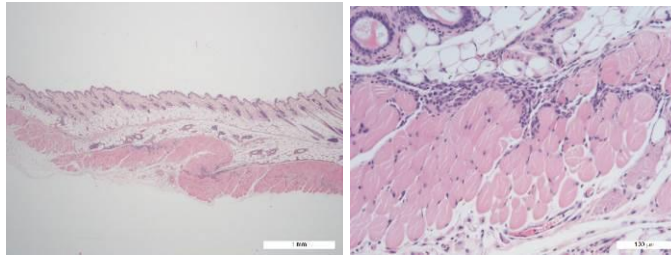
1.6	Lung	Five sections of lung with moderate interstitial pneumonia as above.
	Spleen	One section of normal/reactive spleen.
	Liver	Five sections of normal liver. Small portion of gall bladder with mild inflammatory change of the lamina propria.
	Kidney	Two sections of normal kidney; cortex and medulla.
	Injection site	Strip of skin with changes similar to 1.5, but with the addition of mild diffuse inflammation (granulocytes and macrophages) of the deep adipose tissue beneath the level of the band of mild fibrosis at the deep margin of the muscle block. Additional band of fibrosis/inflammation within the hypodermis above the muscle block.



2.1	Lung	Five sections of lung. Most of the tissue area is normal but with agonal haemorrhage. There are only small areas of interstitial pneumonia in two samples.
-----	------	--



	Spleen	One section of normal/reactive spleen.
	Liver	Five sections of normal liver.
	Kidney	Two sections of normal kidney.
	Injection site	Section of essentially normal skin with central mild band of mixed inflammation immediately above deep muscle block.



2.2	Lung	Five sections of lung with mild to moderate interstitial pneumonia.
	Spleen	Section of normal/reactive spleen and adjacent fragment of normal pancreas.
	Liver	Five sections of normal liver.
	Kidney	Two sections of normal kidney.
	Injection site	Section of normal skin but with light band of early fibroplasia immediately beneath deep muscle block. No inflammatory change.
2.3	Lung	Five sections of lung with mild to moderate interstitial pneumonia.
	Spleen	Section of normal/reactive spleen.
	Liver	Five sections essentially normal liver; mild mononuclear inflammation in one portal area.
	Kidney	Two sections of normal kidney.
	Injection site	Section of normal skin with similar band of fibroplasia at base of deep muscle block.

Table S6: Mouse histopathology from *in vivo* toxicity assay. BALB/c mice were immunized subcutaneously with four sequential doses of SAGE (350 µg in PBS (pH 7.4), n = 6 mice) or PBS (n = 3 mice) at 3 week intervals (2 weeks for the final immunisation). Histopathology results for each tissue analysis of each mouse

General histopathology comments

Group 1 (SAGE) has background changes only in the viscera. Interstitial pneumonia is a common change in laboratory mice, related to housing on dusty bedding. One animal had mild cholecystitis, also regarded as incidental. The major change related to the injection site. Four of six mice had prominent diffuse oedema, microhaemorrhage and moderate inflammation (dominated by granulocytes and macrophages). There was also variable vasculitis/thrombosis

and some focal myositis/myonecrosis of the deep muscle fibres. These animals also had variable amounts of bright eosinophilic, angular (adjuvant?) material deposited at different levels of the skin and associated with surrounding inflammatory cells. This is interpreted as the injected material. Two of the five mice had only mild inflammation and early fibrosis within the adipose tissue beneath the deep muscle block (and in one case also within the hypodermis above this muscle block).

Group 2 (PBS) has the same range of background changes in the viscera, although the lungs of one of these three animals is least affected by interstitial pneumonia. The skin samples show no evidence of active inflammation or deposition of adjuvant material. There is some mild fibroblastic activity at the base of the deep muscle block. It is not clear whether this is a significant pathological change or a background process.

Overall, the most significant changes in these samples are in the skin. There is marked and diffuse inflammation associated with larger quantities of adjuvant material in group 1, but only mild (background?) change in group 2 in the absence of active inflammation or adjuvant material.

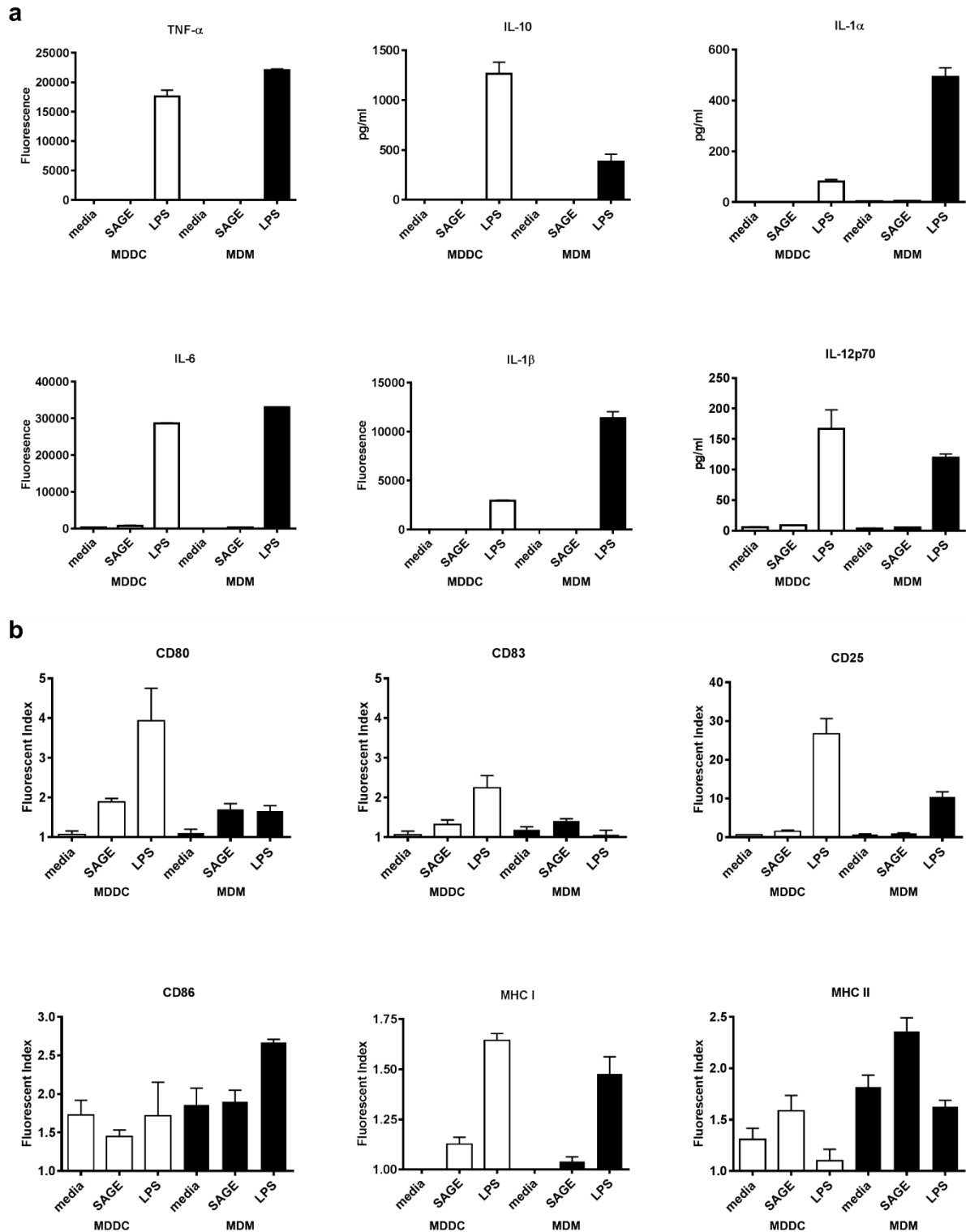


Figure S11: Activation of antigen presenting cells. **a** PBMCs differentiated into MDDCs or MDMs were analysed for cytokine production related to activation or antigen presentation when exposed to parent SAGE or LPS. **b** PBMCs differentiated into MDDCs or MDMs were analysed for expression of surface markers related to activation or antigen presentation when exposed to parent SAGE or LPS. Conditions: parent SAGE at 10 μM in PBS (pH 7.4); LPS at 100 ng ml^{-1} ; $n = 3$ donors.

References

- [1] a) S. J. Draper, B. K. Sack, C. R. King, C. M. Nielsen, J. C. Rayner, M. K. Higgins, C. A. Long, R. A. Seder, *Cell Host Microbe* **2018**, *24*, 43; b) O. Ringel, V. Vieillard, P. Debré, J. Eichler, H. Büning, U. Dietrich, *Viruses* **2018**, *10*, 197.
- [2] G. A. Poland, R. B. Kennedy, I. G. Ovsyannikova, R. Palacios, P. L. Ho, J. Kalil, *Lancet Infect. Dis.* **2018**, *18*, e211.
- [3] K. U. Jansen, A. S. Anderson, *Hum. Vaccines Immunother.* **2018**, *14*, 2142.
- [4] B. Greenwood, *Philos. Trans. R. Soc., B* **2014**, 369.
- [5] S. Plotkin, *Proc. Natl. Acad. Sci. U. S. A.* **2014**, *111*, 12283.
- [6] a) J. Frey, *Vaccine* **2007**, *25*, 5598; b) B. F. Hibbs, E. Miller, J. Shi, K. Smith, P. Lewis, T. T. Shimabukuro, *Vaccine* **2018**, *36*, 553.
- [7] a) M. Pizza, V. Scarlato, V. Maignani, M. M. Giuliani, B. Aricò, M. Comanducci, G. T. Jennings, L. Baldi, E. Bartolini, B. Capecchi, C. L. Galeotti, E. Luzzi, R. Manetti, E. Marchetti, M. Mora, S. Nuti, G. Ratti, L. Santini, S. Savino, M. Scarselli, E. Storni, P. Zuo, M. Broecker, E. Hundt, B. Knapp, E. Blair, T. Mason, H. Tettelin, D. W. Hood, A. C. Jeffries, N. J. Saunders, D. M. Granoff, J. C. Venter, E. R. Moxon, G. Grandi, R. Rappuoli, *Science* **2000**, *287*, 1816; b) R. Rappuoli, *Vaccine* **2001**, *19*, 2688.
- [8] a) C. Maisonneuve, S. Bertholet, D. J. Philpott, E. De Gregorio, *Proc. Natl. Acad. Sci. U. S. A.* **2014**, *111*, 12294; b) J. C. Frei, A. S. Wirchnianski, J. Govero, O. Vergnolle, K. A. Dowd, T. C. Pierson, M. Kielian, M. E. Girvin, M. S. Diamond, J. R. Lai, *J. Virol.* **2018**, *92*.
- [9] A. S. McKee, P. Marrack, *Curr. Opin. Immunol.* **2017**, *47*, 44.
- [10] a) K. T. Gause, A. K. Wheatley, J. Cui, Y. Yan, S. J. Kent, F. Caruso, *ACS Nano* **2017**, *11*, 54; b) D. Qiao, L. Liu, Y. Chen, C. Xue, Q. Gao, H.-Q. Mao, K. W. Leong, Y. Chen, *Nano Lett.* **2018**, *18*, 3007.
- [11] a) S. Hollingshead, I. Jongerius, R. M. Exley, S. Johnson, S. M. Lea, C. M. Tang, *Nat Commun* **2018**, *9*, 1051; b) A. L. Parry, N. A. Clemson, J. Ellis, S. S. R. Bernhard, B. G. Davis, N. R. Cameron, *J. Am. Chem. Soc.* **2013**, *135*, 9362; c) Q. Guo, D. Dasgupta, T. A. Doll, P. Burkhard, D. E. Lanar, *Methods* **2013**, *60*, 242.
- [12] a) J. B. Ulmer, U. Valley, R. Rappuoli, *Nat. Biotechnol.* **2006**, *24*, 1377; b) C. P. Karch, J. Li, C. Kulangara, S. M. Paulillo, S. K. Raman, S. Emadi, A. Tan, Z. H. Helal, Q. Fan, M. I. Khan, P. Burkhard, *Nanomedicine* **2017**, *13*, 241.
- [13] a) L. H. Chen, D. H. Hamer, *JAMA* **2017**, *318*, 1651; b) R. Yaesoubi, C. Trotter, C. Colijn, M. Yaesoubi, A. Colombini, S. Resch, P. A. Kristiansen, F. M. LaForce, T. Cohen, *PLoS Med.* **2018**, *15*, e1002495.
- [14] L. O. De Serrano, D. J. Burkhart, *J. Nanobiotechnol.* **2017**, *15*, 83.
- [15] M. O. Mohsen, L. Zha, G. Cabral-Miranda, M. F. Bachmann, *Semin. Immunol.* **2017**, *34*, 123.
- [16] a) S. Eskandari, T. Guerin, I. Toth, R. J. Stephenson, *Adv. Drug Delivery Rev.* **2017**, *110-111*, 169; b) C. D. Spicer, C. Jumeaux, B. Gupta, M. M. Stevens, *Chem. Soc. Rev.* **2018**, *47*, 3574.
- [17] Y. Hsia, J. B. Bale, S. Gonen, D. Shi, W. Sheffler, K. K. Fong, U. Nattermann, C. Xu, P.-S. Huang, R. Ravichandran, S. Yi, T. N. Davis, T. Gonen, N. P. King, D. Baker, *Nature* **2016**, *535*, 136.
- [18] S. Raman, G. Machaidze, A. Lustig, U. Aebi, P. Burkhard, *Nanomedicine* **2006**, *2*, 95.
- [19] a) Y. Yang, T. Neef, C. Mittelholzer, E. G. Garayoa, P. Bläuenstein, R. Schibli, U. Aebi, P. Burkhard, *J. Nanobiotechnol.* **2013**, *11*, 36; b) Y. Yang, P. Ringler, S. A. Muller, P. Burkhard, *J Struct Biol* **2012**, *177*, 168.
- [20] T. A. Pimentel, Z. Yan, S. A. Jeffers, K. V. Holmes, R. S. Hodges, P. Burkhard, *Chem. Biol. Drug. Des.* **2009**, *73*, 53.
- [21] a) Q. Guo, D. Dasgupta, T. A. Doll, P. Burkhard, D. E. Lanar, *Methods* **2013**, *60*, 242; b) S. A. Kaba, C. Brando, Q. Guo, C. Mittelholzer, S. Raman, D. Tropel, U. Aebi, P. Burkhard, D. E. Lanar, *J. Immunol.* **2009**, *183*, 7268; c) M. E. McCoy, H. E. Golden, T. A. Doll, Y. Yang, S. A. Kaba, P. Burkhard, D. E. Lanar, *Malar. J.* **2013**, *12*, 136; d) S. A. Kaba, M. E. McCoy, T. A. Doll, C. Brando, Q. Guo, D. Dasgupta, Y. Yang, C. Mittelholzer, R. Spaccapelo, A. Crisanti, P.

- Burkhard, D. E. Lanar, *PLoS One* **2012**, 7, e48304; e) C. P. Karch, T. Doll, S. M. Paulillo, I. Nebie, D. E. Lanar, G. Corradin, P. Burkhard, *J. Nanobiotechnol.* **2017**, 15, 62; f) S. A. Kaba, C. P. Karch, L. Seth, K. M. B. Ferlez, C. K. Storme, D. M. Pesavento, P. Y. Laughlin, E. S. Bergmann-Leitner, P. Burkhard, D. E. Lanar, *Vaccine* **2018**, 36, 906.
- [22] N. Wahome, T. Pfeiffer, I. Ambiel, Y. Yang, O. T. Keppler, V. Bosch, P. Burkhard, *Chem. Biol. Drug. Des.* **2012**, 80, 349.
- [23] a) Y. Zimenkov, V. P. Conticello, L. Guo, P. Thiyagarajan, *Tetrahedron* **2004**, 60, 7237; b) N. C. Burgess, T. H. Sharp, F. Thomas, C. W. Wood, A. R. Thomson, N. R. Zaccai, R. L. Brady, L. C. Serpell, D. N. Woolfson, *J. Am. Chem. Soc.* **2015**, 137, 10554.
- [24] T. Sun, H. Han, G. A. Hudalla, Y. Wen, R. R. Pompano, J. H. Collier, *Acta Biomater.* **2016**, 30, 62.
- [25] Y. Zimenkov, S. N. Dublin, R. Ni, R. S. Tu, V. Breedveld, R. P. Apkarian, V. P. Conticello, *J. Am. Chem. Soc.* **2006**, 128, 6770.
- [26] R. R. Pompano, J. Chen, E. A. Verbus, H. Han, A. Fridman, T. McNeely, J. H. Collier, A. S. Chong, *Adv Healthc Mater* **2014**, 3, 1898.
- [27] G. A. Hudalla, J. A. Modica, Y. F. Tian, J. S. Rudra, A. S. Chong, T. Sun, M. Mrksich, J. H. Collier, *Adv Healthc Mater* **2013**, 2, 1114.
- [28] J. M. Fletcher, R. L. Harniman, F. R. Barnes, A. L. Boyle, A. Collins, J. Mantell, T. H. Sharp, M. Antognozzi, P. J. Booth, N. Linden, M. J. Miles, R. B. Sessions, P. Verkade, D. N. Woolfson, *Science* **2013**, 340, 595.
- [29] J. M. Galloway, L. Senior, J. M. Fletcher, J. L. Beesley, L. R. Hodgson, R. L. Harniman, J. M. Mantell, J. Coombs, G. G. Rhys, W. F. Xue, M. Mosayebi, N. Linden, T. B. Liverpool, P. Curnow, P. Verkade, D. N. Woolfson, *ACS Nano* **2018**, 12, 1420.
- [30] M. Mosayebi, D. K. Shoemark, J. M. Fletcher, R. B. Sessions, N. Linden, D. N. Woolfson, T. B. Liverpool, *Proc. Natl. Acad. Sci. U. S. A.* **2017**, 114, 9014.
- [31] a) J. F. Ross, A. Bridges, J. M. Fletcher, D. Shoemark, D. Alibhai, H. E. V. Bray, J. L. Beesley, W. M. Dawson, L. R. Hodgson, J. Mantell, P. Verkade, C. M. Edge, R. B. Sessions, D. Tew, D. N. Woolfson, *ACS Nano* **2017**, 11, 7901; b) J. L. Beesley, H. E. Baum, L. R. Hodgson, P. Verkade, G. S. Banting, D. N. Woolfson, *Nano Lett.* **2018**, 18, 5933.
- [32] B. M. Diethelm-Okita, D. K. Okita, L. Banaszak, B. M. Conti-Fine, *J. Infect. Dis.* **2000**, 181, 1001.
- [33] a) L. Z. Sun, S. Elsayed, T. B. Aasen, T. Van Do, N. P. Aardal, E. Florvaag, K. Vaali, *Scand. J. Immunol.* **2010**, 71, 329; b) B. J. McFarland, A. J. Sant, T. P. Lybrand, C. Beeson, *Biochemistry* **1999**, 38, 16663.
- [34] D. J. Morgan, H. T. C. Kreuwel, S. Fleck, H. I. Levitsky, D. M. Pardoll, L. A. Sherman, *J. Immunol.* **1998**, 160, 643.
- [35] L. de Haan, A. R. Hearn, A. J. Rivett, T. J. Hirst, *Infect. Immun.* **2002**, 70, 3249.
- [36] M. E. Pichichero, *Hum. Vaccines Immunother.* **2013**, 9, 2505.
- [37] a) M. E. C. Lutsiak, D. R. Robinson, C. Coester, G. S. Kwon, J. Samuel, *Pharm. Res.* **2002**, 19, 1480; b) J. Jia, Y. Zhang, Y. Xin, C. Jiang, B. Yan, S. Zhai, *Front. Oncol.* **2018**, 8, 404.
- [38] S. J. Piersma, M. P. P. A. M. Leenaars, L. Guzylack-Piriou, A. Summerfield, C. F. M. Hendriksen, K. C. McCullough, *Vaccine* **2006**, 24, 3076.
- [39] Z.-G. Yang, H.-X. Sun, W.-H. Fang, *Vaccine* **2005**, 23, 5196.
- [40] D. J. Morgan, R. Liblau, B. Scott, S. Fleck, H. O. McDevitt, N. Sarvetnick, D. Lo, L. A. Sherman, *J. Immunol.* **1996**, 157, 978.
- [41] B. J. H. Kuipers, H. Gruppen, *J. Agric. Food Chem.* **2007**, 55, 5445.
- [42] P. Schuck, *Biophys. J.* **2000**, 78, 1606.